Argonne NATIONAL LABORATORY

Advanced Reactor Safeguards & Security

Flow Enhanced Electrochemical Sensor Performance in Complex Salt Systems

Prepared for
US Department of Energy

William H. Doniger, Timothy Kim, Nora A. Shaheen, Nathaniel C. Hoyt

Argonne National Laboratory

September 30, 2025
ANL/CFCT-25/27

Executive Summary

Molten salt reactors (MSRs) have attracted considerable interest as clean sources of electricity and process heat due to their efficiency, passive safety features, and high operating temperatures. Traditional material control and accounting (MC&A) practices in liquid fuel MSRs are challenging because the fissile inventory is not a discrete item, and transmutation and depletion of fuel lead to transient quantities of special nuclear materials. To advance MSR MC&A practices, Argonne National Laboratory developed and optimized robust flow enhanced electrochemical sensors (FEES) and multielectrode array voltammetry sensors (MAVS), which provide accurate near-real-time measurements of actinides in molten salts. FEES are installed directly into MSR flow conduits for inline salt chemistry measurement, while MAVS are deployed in quiescent salt conditions, enabling online species concentration determination in stationary salt vessels. This report summarizes efforts to improve electrochemical sensor technological readiness through (1) sensor testing in complex, high-concentration molten salt systems to demonstrate low uncertainty actinide measurements in MSR-representative solutions and (2) demonstrations of sensor performance in challenging real-world conditions in collaboration with partner MSR institutions.

The work accomplished in FY25 built upon previous achievements and advanced electrochemical MC&A technologies through the development of updated near-real-time electroanalytical approaches for molten salts containing very high concentrations of actinides. These strategies enable safeguarding of fuel fabrication and MSR systems. The approaches were applied to actinide measurements in an engineering-scale salt production system and in a flowing molten salt system containing high concentrations of uranium chloride. To enable accurate high-concentration measurements, voltammetry simulation tools were developed to correct for adverse non-ideal solution effects, such as uncompensated ohmic resistance, in LiCl-KCl-UCl_3 salts with UCl_3 mass fractions as high as 0.72. In salts with UCl_3 mass fractions ranging from 0.55 to 0.72, the mean absolute relative error of the initial UCl_3 concentration measurements was 4.0 % when the data was corrected for ohmic resistance. Later tests involving the addition of nine surrogate fission products demonstrated that the voltammetric approach for measuring uranium chloride concentrations in chloride salts was independent of the concentration of surrogates for relevant fission products such as Ce, Nd, La, Sm, Pr, Y, Ba, Sr, and Cs. Furthermore, when the chloride form of these surrogates were added to a salt containing 72.3 wt% UCl_3, the mean absolute relative error for the UCl_3 concentration measurements was only 0.8 %.

Argonne National Laboratory also successfully demonstrated electroanalytical tools in representative testing environments at partner MSR vendors. In FY24, two FEES sensors were operated for over 900 hours in a 2LiF-BeF_2 salt test loop at Kairos Power, LLC. In FY25, MAVS sensors were tested in stationary chloride salts containing simulated $CrCl_2$ corrosion products at TerraPower, LLC. While these experiments were non-radiological and focused on system health diagnostics, the strategies that were applied served to demonstrate that accurate measurements can be successfully taken remotely within varied equipment designs.

In total, our work conducted over the past five years for the ARSS program has served to enable the development of new safeguards-relevant monitoring tools along with the creation of several testing platforms that supported sensor assessments in real-world conditions. Beyond that, we were also able to develop automation capabilities that permitted complex combined flow scenarios with synchronized sensor operations. This combination of activities substantially improved extant capabilities for achieving MC&A and safeguarding of special nuclear material (SNM) in molten salt systems.

CONTENTS

Figures

Acronyms and Abbreviations

ANL	Argonne National Laboratory
CA	Chronoamperometry
CV	Cyclic Voltammogram
DOE	US Department of Energy
FEES	Flow-enhanced Electrochemical Sensor
MAVS	Multielectrode Array Voltammetry Sensor
MALS	Multielectrode Array Level Sensors
MC&A	Materials Control and Accounting
MFC	Mass Flow Controller
MFR	Measured Flow Rate
MFIT	Modular Flow Instrumentation Testbed
MSR	Molten Salt Reactor
PT	Pressure Transducer
slpm	Standard Liters Per Minute
SNM	Special Nuclear Material
TC	Thermocouple

Acknowledgements

This report serves as the deliverable for Milestone M3RS-25AN0401052 that is a part of Work Package RS-25AN040105 (*Flow-Enhanced Sensors for MSRs – ANL*).

This report was produced under the auspices of the US DOE Office of Nuclear Energy's Advanced Reactor Safeguards and Security Program, Dr. B. Cipiti, National Technical Director and D. Warner, Program Manager.

This work was conducted at Argonne National Laboratory and supported by the U.S. Department of Energy, Office of Nuclear Energy, under Contract DE-AC02-06CH11357.

Advanced Reactor Safeguards and Security Program

FLOW ENHANCED ELECTROCHEMICAL SENSOR PERFORMANCE IN COMPLEX SALT SYSTEMS

1. Introduction

In support of the DOE Department of Nuclear Energy's Advanced Reactor Safeguards & Security (ARSS) program, Argonne National Laboratory has developed novel sensors, versatile testbeds, and salt synthesis systems to support the development of material control and accountancy (MC&A) technologies for liquid-fueled molten salt reactors (MSRs). It is likely that a liquid-fuel MSR with non-discrete special nuclear materials (SNM) items will require a formal MC&A plan as part of its licensing strategy [1]. Molten chloride fast reactor concepts, for example, may operate with a molten salt containing weight fractions of UCl_3 greater than 70 wt %. The complex, high-concentration molten salt system presents new challenging conditions that require novel electroanalytical approaches. The objective of work completed in FY25 was to test electrochemical sensors in complex, high-concentration molten salt systems to demonstrate low uncertainties for actinide measurements in MSR-representative solutions. These sensor capabilities were applied to safeguard-relevant scenarios, including both the synthesis of highly-loaded chloride salts and flowing salt systems to demonstrate the efficacy of electroanalytical safeguard tools. Alongside these developmental activities, Argonne coordinated with MSR vendors to deploy sensors to their facilities and equipment.

MSRs present challenging conditions that make it difficult to design and operate robust monitoring tools. Liquid fuel MSRs with large fissile inventory and transient quantities of SNM due to transmutation and depletion of fuel make material balance methods challenging. Detection of materials loss using traditional statistical tests is projected to require at or above current state-of-the-art destructive analysis levels of precision. To mitigate the number of required control elements — tamper-safing and surveillance, for example — the number of penetrations to the control boundary should be minimized [2]. As such, new nondestructive monitoring approaches are under development, including electrochemical sensors [3]–[6], in-line spectroscopic sensors [7], gamma and neutron measurements [8], and alpha spectroscopy [9]. The goal of our research is to develop in-line and on-line electrochemical tools that offer near real-time measurements and enable MSR vendors to achieve the regulatory requirements for material accountancy (10 CFR 74) as part of their MC&A plan.

Voltammetry approaches are well-established techniques for quantifying dilute actinides in molten salts but have had limited application in quantifying highly loaded actinides in molten salts. Voltammetry has been used to quantify actinides in dilute mixtures of uranium chloride [10]–[27] and uranium fluoride.[28]–[34] Previously, there have been no voltammetric studies of chloride salts with UCl_3 weight fractions relevant to molten chloride fast reactors (e.g., > 12.5 wt %). Voltammetric analysis of high-concentration actinide salt mixtures presents several challenges, including high currents generated by the abundant reactants and non-ideal solution effects, such as ohmic resistance. Typically, species concentrations can be obtained from a set of thermodynamic and kinetic parameters, such as species reduction potentials, temperature, and species diffusion coefficients; however, the presence of these solution characteristics requires careful treatment. To close these gaps, we have developed an electroanalytical approach and correction factors based on numerical simulations of voltammetry responses. Utilizing a multielectrode array voltammetry sensor (MAVS), shown in Figure 1(a), the correction factors were demonstrated agnostic of electrochemical cell geometry and produced consistent voltammetry peak current results when correcting for varying amounts of ohmic resistance. This approach enables accurate in situ measurements of uranium concentrations in highly loaded fuel salts.

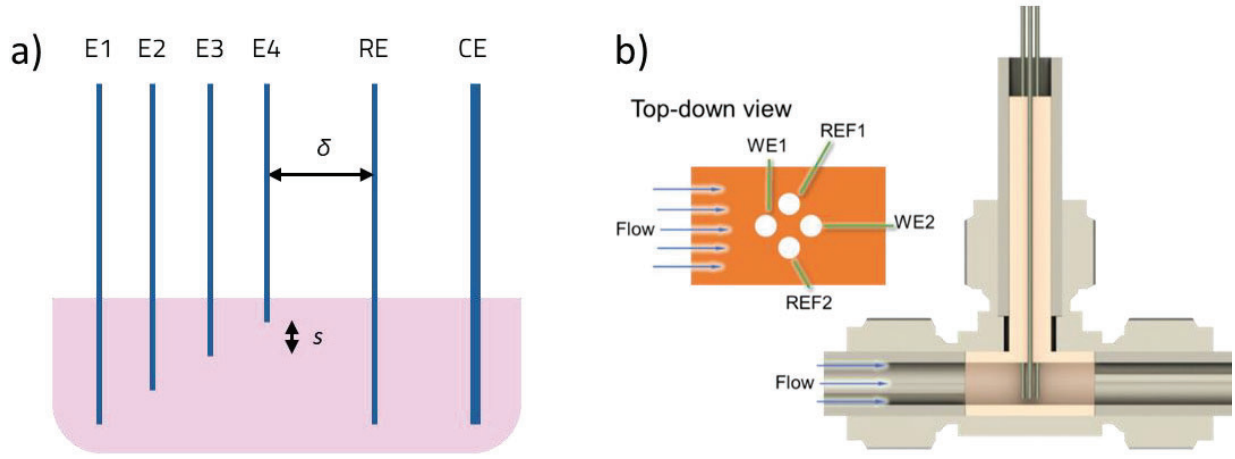

Figure 1. Schematic of (a) the multielectrode array voltammetry sensor and (b) the flow-enhanced electrochemical sensor.

The high flow velocities encountered in an MSR are an additional significant challenge for salt chemistry sensors. Argonne has developed flow enhanced electrochemical sensors (FEES), which make use of hydrodynamic electrochemical approaches to measure the concentrations of species in the molten salt. A diagram of a FEES inserted in-line with the process stream is shown in Figure 1(b). Unlike voltammetry sensors in quiescent salt conditions, FEES operate using steady signals as the flow of salt provides a constant flux of analytes to the electrode surface. The use of steady signals eliminates several issues that can distort dynamic electroanalytical waveforms, such as uncompensated resistance and kinetic effects. In previous years, FEES have been demonstrated in salt containing up to 5 wt% UCl_3 [6]. In FY25, FEES sensors were operated in higher concentration salts containing up to 43.4 wt% UCl_3.

This report summarizes the activities conducted during FY25 to develop electrochemical safeguards tools that can effectively be deployed as part of an MSR vendor's MC&A plan. We have developed an electroanalytical approach that enables accurate in situ measurements of actinide concentrations in these highly loaded fuel salts. Electrochemical sensors have been used to validate methods for the synthesis of high-concentration uranium chloride molten salts. Online electrochemical sensors were then applied in safeguard-relevant scenarios as a part of large-scale salt synthesis activities. An in-line flow enhanced electrochemical sensor (FEES) was then deployed in a high-concentration molten chloride salt. In parallel, voltammetry sensors were deployed in preliminary stationary salt experiments at TerraPower, LLC in preparation for planned loop operations. Descriptions of all these activities are included in the following sections.

1. Experimental Systems Developed for the ARSS Program

Over the last five years, Argonne created numerous molten salt systems under the ARSS program to support the development of safeguards practices and tools for molten salt reactors. The newly developed technologies and equipment included novel sensors, testbeds for sensor performance testing, and engineering-scale purification systems to produce a variety of MSR-relevant salts. Figure 2 shows a rendering of some of these systems installed into the Molten Salt Flow Systems glovebox that was refurbished and brought online at the start of the project in FY21. The salt flow systems include the modular flow instrumentation testbed (MFIT) which is a versatile system for studying in situ sensor performance during safeguards-relevant scenarios. In FY25, to synthesize the large quantities of highly loaded uranium-bearing chloride salts necessary for electroanalytical studies, bench-scale and engineering-scale salt production systems were designed and operated. These apparatuses have been used to enable the development of a suite of molten salt sensors, including flow enhanced electrochemical sensors (FEES), multi-electrode array voltammetry sensors (MAVS), and multielectrode array level sensors (MALS). Versatile software and instrumentation were developed for the integration of these systems. These combined systems enable performance assessments and safeguards scenario studies for a variety of tools and approaches. Detailed descriptions of the individual subsystems and apparatus are included in the subsections below.

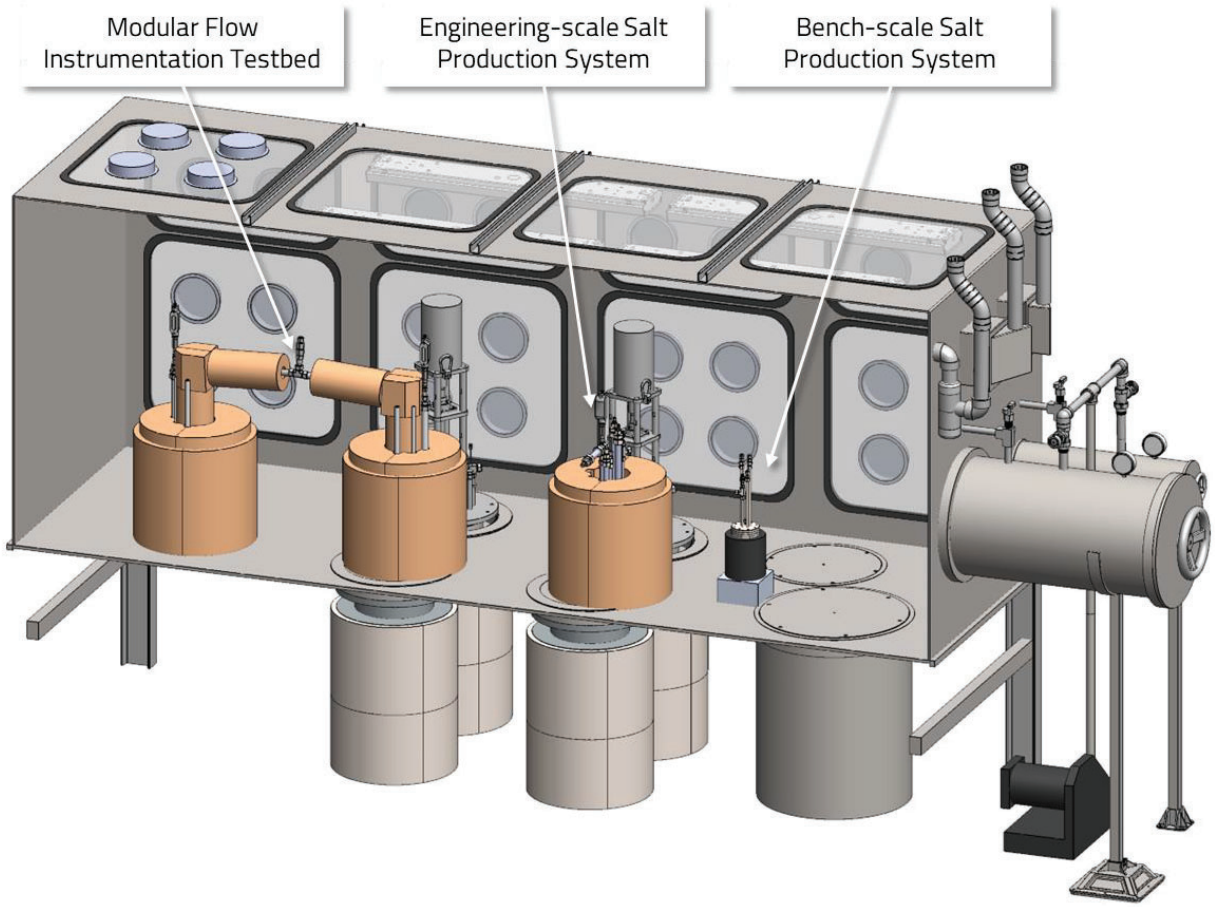

Figure 2. Rendering of Argonne's Molten Salt Flow Systems Glovebox along with installation location for various experimental systems developed for the ARSS program.

1.1. Testbeds for Operational Assessments of Sensors in Flowing Salts

Three forced convection molten salt flow systems, called MFITs, were developed over the course of ARSS activities over the past five years. These flow systems are intended to be modular, versatile, and provide well-controlled flow conditions. These MFITs make use of pressurized gas or applied vacuum to facilitate the salt flow and have adopted two separate configurations. The largest system is the Dual Tank MFIT that initiates flow via tank-to-tank transfers, while two smaller systems, called Miniature-MFITs, achieve flow through a vertical arrangement where flow is withdrawn from a salt crucible. These systems have successfully been tested with both radiological and non-radiological gloveboxes. The modularity of the MFIT design means that combinations of these configurations can be used to achieve desired salt transport characteristics and accommodate various quantities of molten salt ranging from several hundred milliliters to many liters of salt. Each of these systems were designed with careful consideration for operations, and numerous safety devices including relief valves, gas cut-off valves, a pneumatically actuated pressure relief valve, and a bubbler were included in the final construction. More details of each of these three flow systems are included below.

1.1.1. Dual Tank Radiological MFIT

The dual tank MFIT is an engineering-scale forced convection molten salt flow system. Figure 3 shows a schematic and image of the system inside of a radiological glovebox. The system consists of two vessels connected by a molten salt transfer line, and it has the capacity for large quantities of radiological salts up to 10 liters. As shown in the schematic, the MFIT has numerous ports in each tank that enable rapid installation and modification of new sensor designs and configurations. The flow of the molten salt is controlled by applying pressurized argon gas (<15 PSIG) to one of the two tanks. A flow enhanced electrochemical sensor (FEES) is installed in the center of the transfer line. A multielectrode array voltammetry sensor (MAVS) is installed in one vessel. A multielectrode array level sensor (MALS) is installed in the other vessel. In FY24, the dual tank MFIT was operated with 2.1 kg of $MgCl_2$-KCl-NaCl-UCl_3 containing 3 wt % UCl_3.

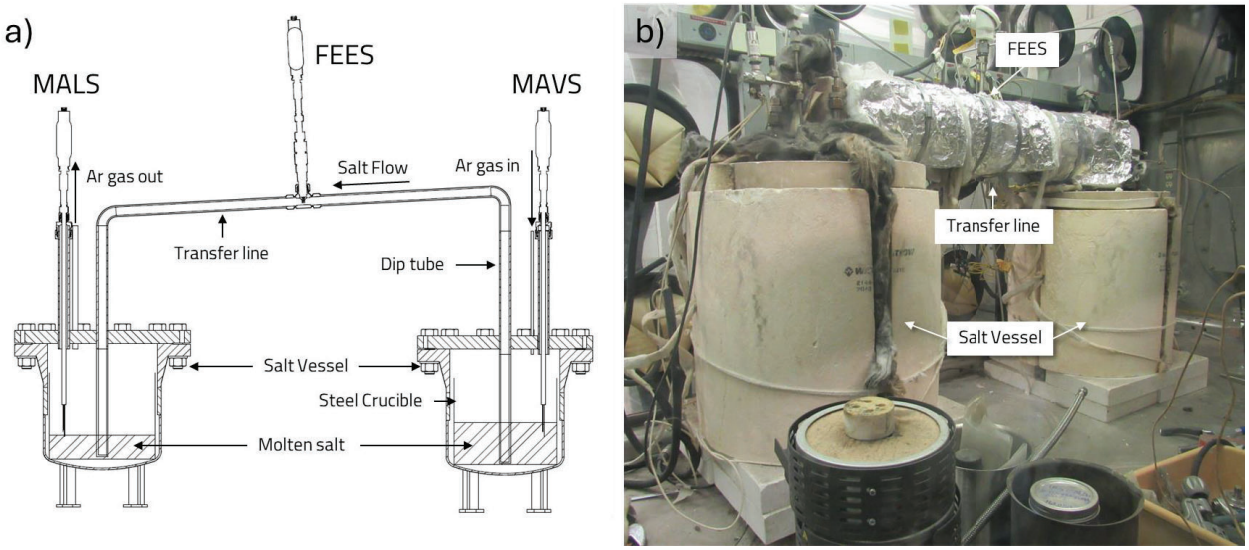

Figure 3. The dual tank modular flow instrumentation testbed (a) schematic and (b) system assembled in an inert atmosphere radiological glovebox.

1.1.2. Non-Radiological Miniature-MFIT

The Miniature-MFIT is a second configuration of the engineering scale MFIT that also enables studies of flowing molten salt. This system was first operated in FY23 and was built to enable rapid testing with non-radiological salts. In FY24, the Miniature-MFIT was successfully tested with non-radiological molten salts containing corrosion products, such as $CrCl_2$ and $FeCl_2$ [6]. The schematic of this system is shown in Figure 4(a). The Miniature-MFIT and the vacuum system used to operate it are shown in Figure 4(b). The advantage of this Miniature-MFIT configuration is the ability to work with 200 mL to 1 L of salt and to achieve sustained slow flow velocities of less than one liter per minute.

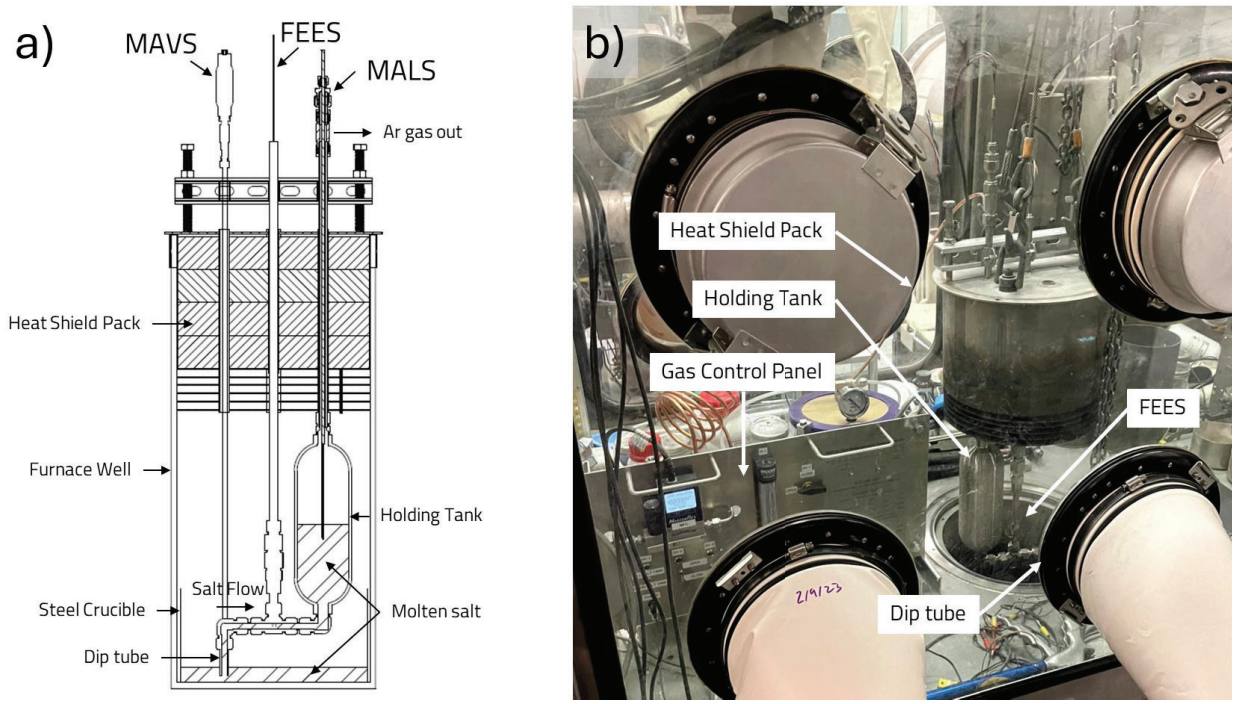

Figure 4. The non-radiological miniature-modular flow instrumentation testbed (a) furnace well schematic and (b) installation into a glovebox furnace well.

1.1.3. Radiological Miniature-MFIT for High-Concentration Fuel Salts

The radiological Miniature-MFIT is another configuration of the engineering scale MFIT that enables studies of flowing molten salt. The advantage of the Miniature-MFIT configuration is the ability to work with 200 mL to 1 L of salt and to achieve sustained slow flow velocities less than a liter per minute. In FY25, the radiological Miniature-MFIT was successfully tested in LiCl-KCl-UCl_3 with 43.4 wt% UCl_3 at 550 °C. The schematic of this system is shown in Figure 5(a). In FY25, the MFIT for radiological salts was reconfigured into a Miniature-MFIT, as shown in Figure 5(b) to conserve radiological materials during the study of highly loaded uranium-bearing salts. The Miniature MFIT can either be operated using a vacuum system, as was demonstrated in FY24 with the non-radiological salts, or with compressed argon gas, provided adequate pressure safety controls in place in the radiological glovebox.

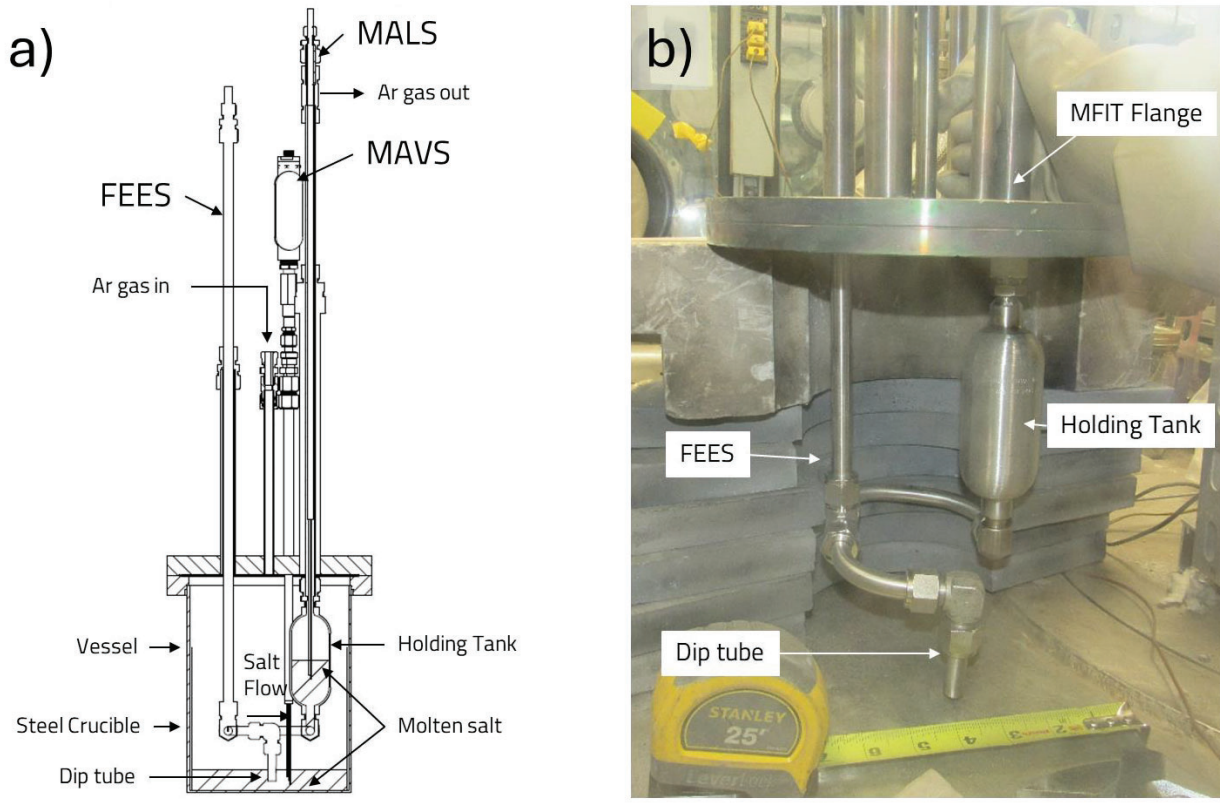

Figure 5. The radiological miniature-modular flow instrumentation testbed (a) furnace well schematic and (b) in a radiological glovebox.

1.2. Salt Production Systems

To facilitate sensor assessments in complex, highly loaded actinide-bearing salts in the MFIT systems, chlorination methods for the preparation of large quantities of high-concentration uranium-bearing salts (>30 wt % U) were developed. As shown in Figure 6, bench-scale experiments were first carried out in a sealed vessel heated by an electro-melt furnace in a glovebox. The vessel contained ports for electrochemical sensors, a thermocouple, a gas inlet and a gas outlet. Compressed argon was used as a process gas and was controlled by a mass flow controller. Chlorination experiments were carried out at 740 °C. Following the successful demonstration of the bench-scale salt production system, an engineering-scale uranium chlorination system was constructed to enable production of multi-kilogram quantities of high-concentration uranium chloride salts for sensor development and testing. In Figure 6, this system is a scaled-up version of the bench-scale uranium chlorination system and shares many design elements with the MFIT. A vessel was constructed that included ports for the chemical reagents, the process gas, a salt sampling system, a byproduct removal system, and electroanalytical sensors. This larger purification vessel can accommodate up to 5 liters of salt.

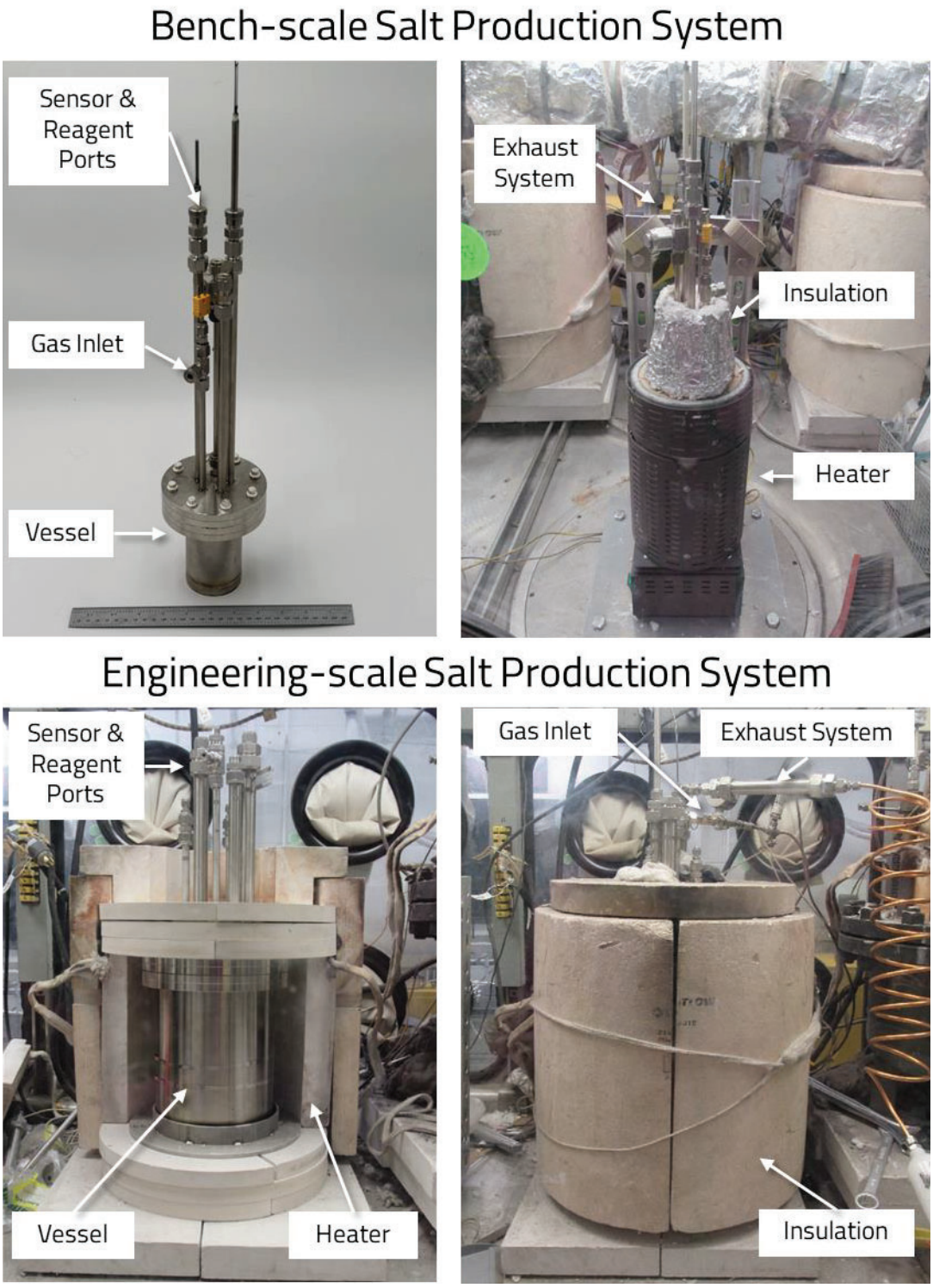

Figure 6. Bench-scale salt production system vessel (top left) and operating in a radiological glovebox (top right). The engineering-scale salt production system partially assembled (bottom left) and operating (bottom right) in a radiological glovebox.

1.3. Multimodal Monitoring Tools

A suite of multimodal sensors were developed, assessed, and deployed as part of this research to enable measurements of the concentrations of species within highly loaded uranium-bearing molten salts. A list of currently installed sensors is included in the section below.

1.3.1. Flow Enhanced Electrochemical Sensors

Flow enhanced electrochemical sensors make use of hydrodynamic electrochemical approaches to measure the concentrations of species in the molten salt [35]. The flow of salt provides a constant flux of analytes to the electrode surface. Unlike voltammetry sensors, FEES operate using steady signals. The use of steady signals eliminates several issues that can distort dynamic electroanalytical waveforms, such as uncompensated resistance and kinetic effects. Figure 1(b) shows a schematic of FEES. The sensor consists of multiple electrodes inserted into the process stream. At least two electrodes are used, including an upstream working electrode (WE) and a quasi-reference electrode (QRE). A fifth electrode or the vessel tube itself may be used as the counter electrode (CE).

As derived in previous work [35], for soluble-soluble reactions such as U^{3+}/U^{4+}, the electroanalytical formulas that are used to convert measured currents into concentrations take the form

$$i = \beta Q^n \Delta C \quad [1]$$

$$\beta = \frac{(\pi/4)^{1-m} d D_i z F k S c^{1/3}}{\rho} \left(\frac{\rho}{\mu d_0}\right)^m \quad [2]$$

Here, F is Faraday's constant, z is the number of electrons associated with the charge transfer reaction, d is the electrode diameter, and M is molar mass of the species of interest, D_i is the diffusion coefficient of the species of interest, Sc is the Schmidt number of the dissolved species within the molten salt ($Sc=D_i/v$), ρ is the salt density, and k and m are values taken from mass transfer correlations associated with specific geometries. ΔC is the difference in species concentration between the bulk fluid and the surface of the electrode. For limiting current conditions when the concentration at the electrode surface falls to zero, ΔC is equal to the bulk concentration of the species of interest. Figure 7 depicts the expected current response to a large anodic applied potential. Full details underpinning the mathematical modeling of these sensors is included in earlier work, along with similar formulas for soluble-insoluble reactions [35]. Figure 7 shows the typical current response to an applied potential sufficient to oxidize U^{3+} to U^{4+} as the fluid flows past a FEES sensor.

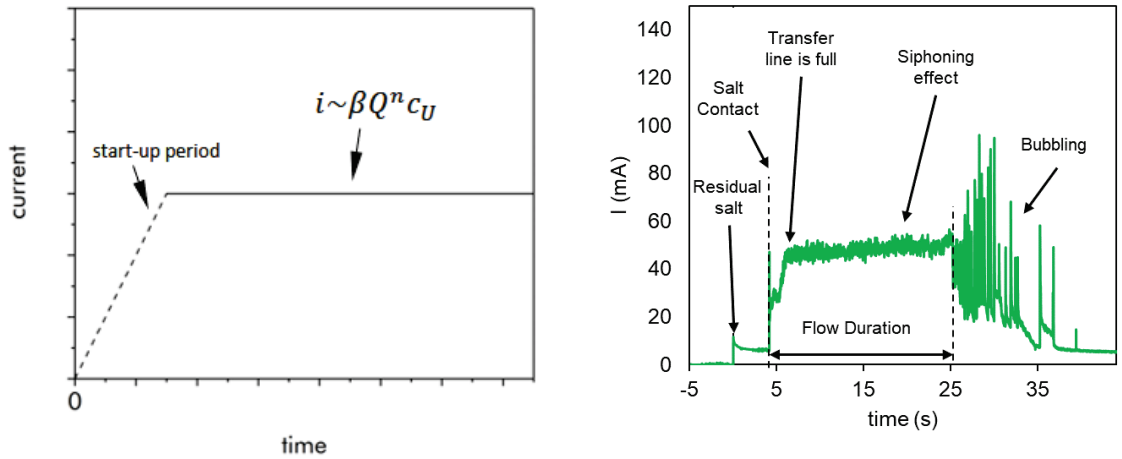

Figure 7. Flow enhanced electrochemical sensor current response at a mass flow rate controller setpoint of 3 L min^{-1} [6].

1.3.2. Multielectrode Array Voltammetry Sensors

Multielectrode array voltammetry sensors (MAVS) were also developed and deployed to facilitate additional measurements of actinides in representative fuel salts. Figure 1(a) depicts a diagram of a MAVS. In quiescent conditions, a dynamic electrical signal is typically applied to the working electrode, which results in a dynamic current response from the salt. The original MAVS concept was developed under the MPACT program for fuel reprocessing salts [4]. One advantage of this multielectrode array approach is the ability to self-validate the sensor immersion depth. Comparison of the current response from each electrode in the array enables near-real-time quantitative analysis.

Key systems have been engineered to remotely operate the MAVS. A Gamry Interface 5000E potentiostat is used for all voltammetric and FEES sensor measurements. In FY25, specialized MAVS multiplexer units, shown in Figure 8, were designed and built for deployment both at Argonne National Laboratory and at partner MSR vendors to sequentially connect the potentiostats to the MAVS and FEES sensors.

Figure 8. Picture of a multielectrode array voltammetry sensors (MAVS) and multiplexer system.

MAVS that were used for low concentration actinide salt applications (<5 wt% UCl_3) consisted of four 1 mm diameter tungsten electrodes that were positioned with a 5 mm stagger relative to one another. In the MFITs, the counter electrode is the vessel wall, and the reference electrode is a tungsten quasi-reference electrode. For high-concentration actinide salts, a smaller sensor surface area was desired to limit the current response from the highly concentrated species. The MAVS sensor for high-concentration actinide salt measurements therefore, consisted of four 0.5 mm diameter tungsten electrodes that were positioned with a 3 mm stagger relative to one another. The counter electrode (CE) was either a 2 mm tungsten electrode or the vessel wall. The quasi-reference electrode typically consisted of a 0.5 mm diameter tungsten wire.

1.3.3. Multielectrode Array Level Sensors

Independent knowledge of the flow rate is crucial for sensor calibrations and the development of high-fidelity flow measurements using electrochemical sensors. Multielectrode array level sensors for molten salts previously developed [6] were deployed for verification of fluid flow MFIT systems. The salt level sensor pictured in Figure 9, consisted of a continuity measurement device connected to an array of electrodes spaced vertically in 5mm increments. As depicted in the diagram in Figure 9(c), the level sensor measured the continuity between the salt tank and the four electrodes in the sensor. When the salt touched an electrode in the sensor, a circuit between the electrode and the salt tank was completed by the salt. The continuity measurement device measured the voltage generated by the small current (<1 μA) which was allowed to flow between the electrode and salt tank when the salt was touching the electrode. In FY25, the MALS were upgraded to communicate via Bluetooth to a device connected to the control computer. Software was used to calculate the change in fluid level in the salt tank with respect to time. Figure 10 shows the salt level and fluid flow rate displayed in real-time. A linear curve fit gives the change in height with respect to time. The software can be calibrated for vessels of various internal diameters, enabling the sensor to be deployed in a variety of testing conditions. Work in FY24 showed that the improved flow rate measurements provided by the MALS system enable improved consistency and lower uncertainty for concentration measurements using the FEES sensors.

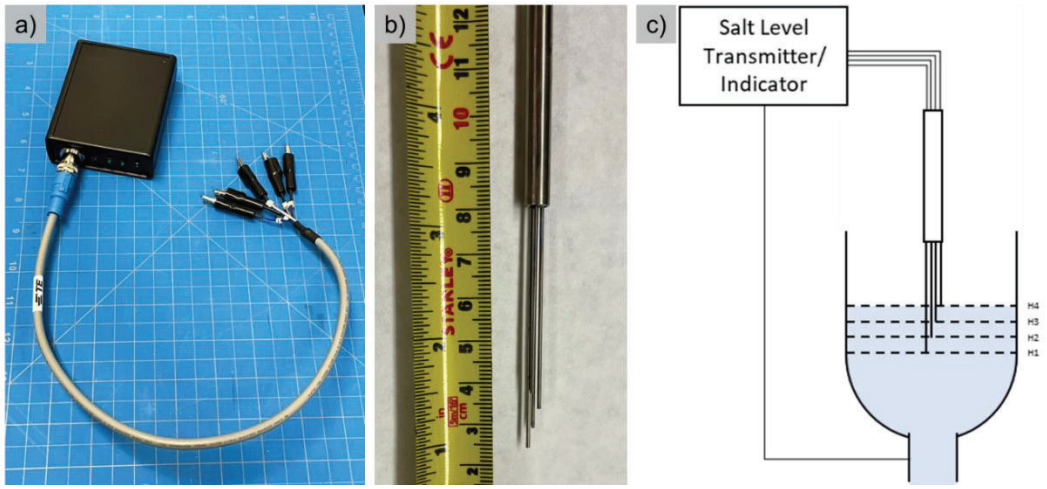

Figure 9. Mini-MFIT salt level sensor (a) continuity measurement device, (b) electrode array sensor, and (c) diagram of salt level sensor placement in the MINI-MFIT salt tank [35].

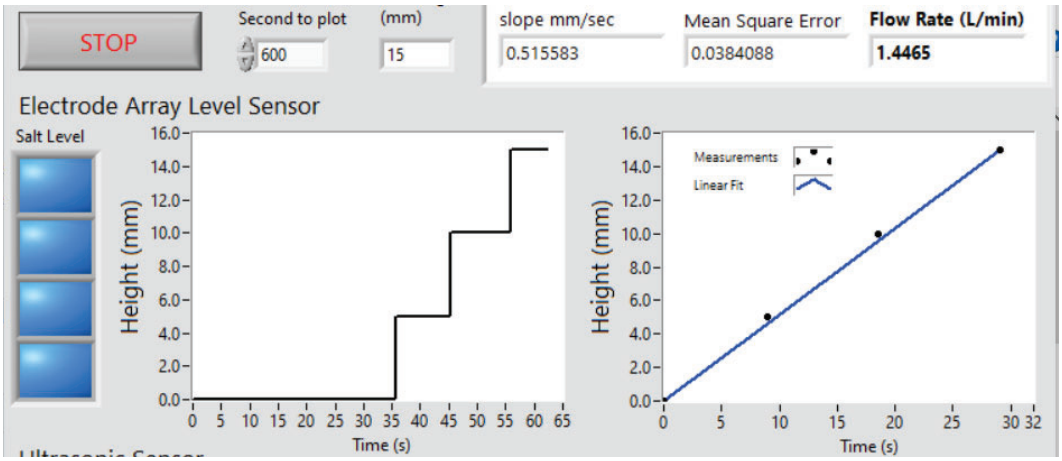

Figure 10. Multielectrode array level sensor (MALS) digital interface software [35].

1.4. Software and Instrumentation

Process automation software has been vital to the operation of engineering-scale flowing salt systems and has facilitated remote operation of electrochemical sensors both at Argonne National Laboratory and at MSR vendors. ILEX Automation© software, shown in Figure 11, was developed under this project to facilitate high-throughput experimentation and to enable sensor deployments to industry. Written in National Instruments LabVIEW™, this versatile framework is used to control FEES and MAVS remotely using multiplexer instrumentation. The software facilitates programmable process controls that can easily be tailored to suit various configurations of the MFIT. Modules, such as the level sensor module, enable real-time analysis of fluid flow rate. The application has been deployed at four locations for remote sensor operations.

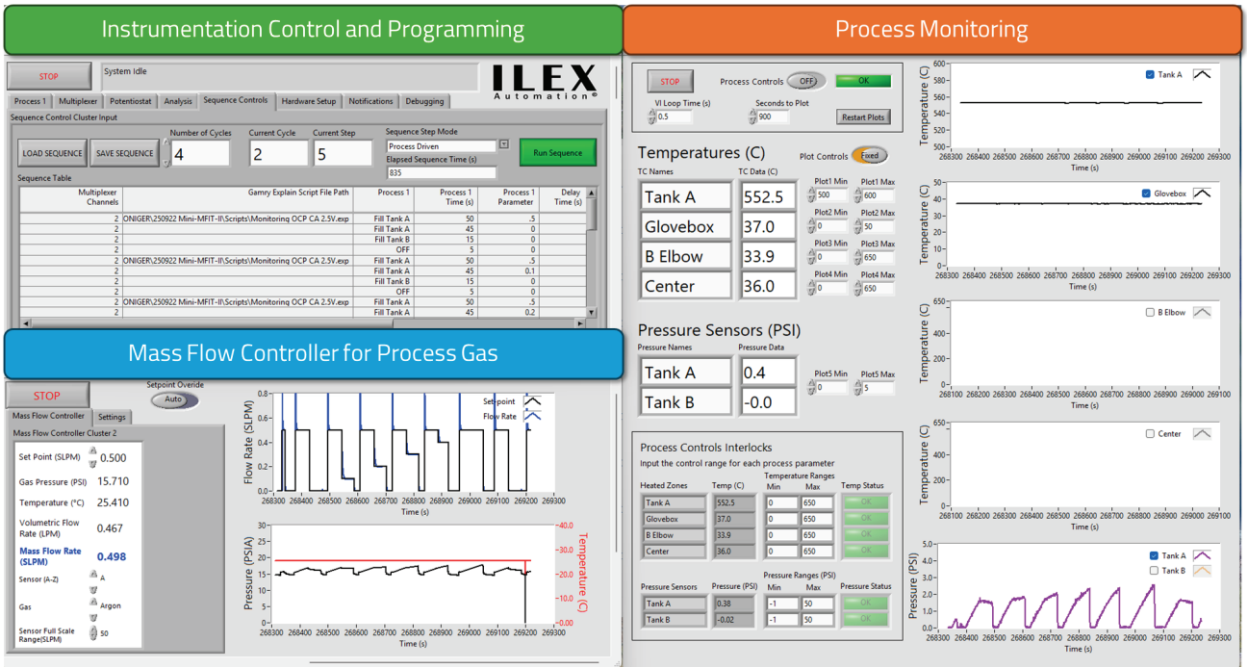

Figure 11. ILEX Automation© Software for control of MFIT, electroanalytical devices, and multiplexers.

All MFIT configurations are instrumented with an array of sensors for process monitoring, including mass flow controllers, thermocouples, and pressure transducers. Figure 12 depicts signals acquired during multiple salt transfers at various mass flow controller setpoints in the radiological Miniature-MFIT. Salt flow is induced by passing Ar gas at a set mass flow rate to pressurize the vessel. The pressure of the vessel rises slowly at the initial flow rate of 0.5 L min^{-1}. The initial flow rate is used to fill the horizontal section containing the FEES before conducting measurements. Following the initial step, the mass flow controller is set to the flow rate of interest and FEES measurements are initiated programmatically. The temperature of the salt in the vessel was monitored with a thermocouple. These sensors offer important diagnostic tools to ensure high-quality salt flow experiments and FEES sensor measurements.

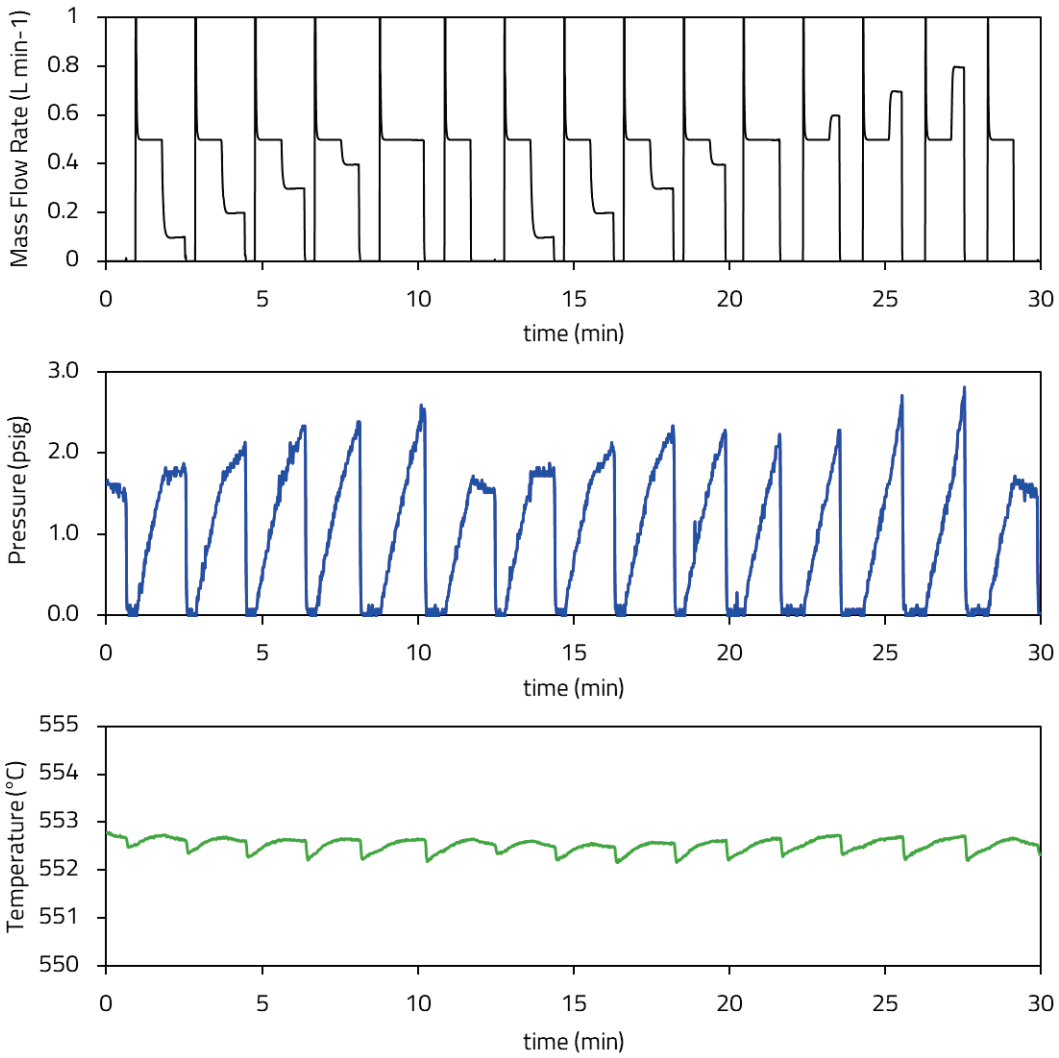

Figure 12. Modular flow instrumentation testbed mass flow controller, pressure transducer, and salt temperature measurements during typical salt transfers at various mass flow controller setpoints.

2. Development of Updated Voltammetry Techniques for Complex High-Concentration Actinide Salts

Throughout the entirety of the ARSS project, Argonne has developed new voltammetry approaches to enable improved near-real-time monitoring and safeguarding of complex actinide-bearing molten salts. Work in previous years primarily focused on relatively low-concentration salts [6], [36], but new techniques for ultra-high concentration salts were pursued starting in FY24. Quantification of the composition of high-concentration salts (i.e., >40wt% U, >70% UCl_3) is needed for chloride fast reactors where the concentrations of actinides are extremely high. As such, the objectives of the voltammetry research were to (i) accurately quantify actinides leveraging numerical simulations tools to account for large currents generated by the analyte and solution effects, and (ii) demonstrate uranium chloride quantification at very high concentrations in the presence of surrogate fission products.

In FY25, voltammetry measurements were conducted in stationary LiCl-KCl-UCl_3 with UCl_3 concentrations between 4.1 mol/L and 6.7 mol/L (55-72 wt%). A detailed analysis of this research can be found in [37]. Voltammetric analysis of these salts generates high currents due to the abundance of reactants. This, combined with uncompensated ohmic resistance, has been observed to cause deviation of voltammetry data from theory in aqueous solutions [38]–[40] and in salts containing high concentrations of UCl_3.[20]–[21] The utilization of positive feedback IR_Ω compensation is often used to mitigate the effects of uncompensated ohmic resistance. However, this approach is typically limited to 90% of the total ohmic resistance and unlikely to be suitable for industrial applications [5]. Recent works by Hoyt et al. [20] and Shaheen et al. [41] used digital simulations to correct for ohmic resistance, R_Ω, in voltammetric measurements. Using similar correction factors produced by theory-based numerical simulations, the research this year aimed to demonstrate that, even for highly concentrated salts, challenges presented by ohmic resistance and non-idealities can be overcome in MSR-relevant salts.

Experiments were conducted in an inert argon atmosphere glovebox which maintained the concentration of oxygen and moisture below 5 ppm. The salts were melted in a binder-free boron-nitride crucible (99% pure) heated in an electro-melt furnace. Ampule grade eutectic LiCl-KCl (58.2-41.8 mol %) with a 99.99% trace metals basis was obtained from Sigma-Aldrich. The salt was baked at 250 °C for 24 hours prior to melting. LiCl-KCl-UCl_3 with 72.3 wt % UCl_3 was previously produced using depleted uranium via a cadmium chlorination process [42]. The salt was diluted at temperature with the LiCl-KCl eutectic salt to obtain a range of actinide concentrations. Table 1 summarizes the composition of the LiCl-KCl-UCl_3 salts measured in this study. The concentration of U in the LiCl-KCl-UCl_3 (72.3wt% U) mother batch was confirmed by ICP-MS. Concentrations for the diluted salts (e.g., 66.6 wt%, 60.8 wt%, etc.) were based on process knowledge. To obtain the UCl_3 diffusion coefficient, the molarity was calculated by assuming an ideal mixing density model [43]. It was assumed that the ideal mixing density model was sufficient to approximate the density at high concentrations and that the error in the density measurement principally contributed to the error in the measured diffusion coefficient. The molarity of UCl_3 in the salts investigated ranged from 4.1 mol/L to 6.7 mol/L. Henceforth, the salt compositions are referred to by their calculated molarity.

Table 1. Concentration, density and molarity of UCl_3 in LiCl-KCl-UCl_3 salts at 550 °C.

UCl_3		ρ_{calc}	M
wt %	mol %	g/mL	mol/L
72.3	29.8	3.2	6.7
66.6	24.4	3.0	5.7
60.8	20.1	2.8	4.8
57.9	18.2	2.7	4.5
55.0	16.5	2.6	4.1

Comparison of the eutectic LiCl-KCl and the 6.7 mol/L UCl_3 salts with cyclic voltammetry (CV), as shown in Figure 13, demonstrated the influence that uranium chloride has on the usable potential range and redox behavior of the salt. Reaction *d'* corresponds to the oxidation of Cl^- and was selected as the internal reference reaction. The approximate redox potential of *d'* was measured by extrapolation of the oxidation curve to the x-axis. Reaction *a*/*a'* corresponded to the Li/Li^+ redox reaction. In the 6.7 mol/L UCl_3 salt, reaction *b/b'* was the U^{3+}/U^0 reaction, and reaction *c/c'* corresponded to the U^{3+}/U^{4+} reaction. Due to the well-behaved nature of soluble-soluble reactions and the absence of electrode area growth effects, the oxidation of U^{3+} to U^{4+} in reaction *c* was selected as the best candidate for quantitative voltammetry analysis [6].

The solution effects, such as ohmic resistance, were investigated by changing the geometry of the electrochemical cell. As shown in Figure 1(a), the horizontal distance, δ, between the working electrode and reference electrode was controlled to achieve different results. In Figure 13, the green and blue voltammograms show the current response to the same potential scan rate when δ equals 1 mm and 20 mm, respectively. As expected, the increase in δ produced higher uncompensated resistance which led to the concomitant broadening of the potential difference between the *c/c'* peak potentials. This was accompanied by a decrease in the magnitude of the peak current.

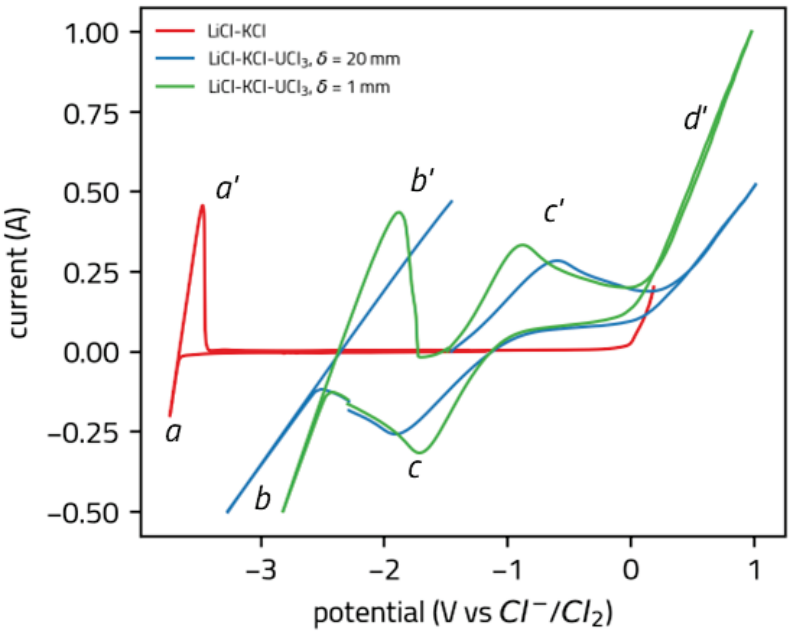

Figure 13. Cyclic voltammograms of LiCl-KCl eutectic and LiCl-KCl-UCl_3 (6.7 x 10^{-3} mol/cm^3 UCl_3) using two cell configurations at 550 °C. The working electrode is the deepest electrode (E1) with a surface area of 0.15 cm^2. The scan rate is 3 V s^{-1}.

For a reversible soluble-soluble reaction, the peak current is expressed by the Randles-Sevcik equation.[44]–[45]

$$I_p = 0.446nFAC\sqrt{\frac{nFvD}{RT}} \quad [3]$$

Here, n is the number of electrons transferred in the reaction, A is the surface area of the electrode, C is the concentration of the reacting species, R is the gas constant, and T is temperature. Voltammetry approaches that correct for these peak distortions must be implemented to obtain reliable electrode surface area and concentration measurements. To address this, CVs were simulated using the Coefficient Form Partial Differential Equation interface in COMSOL Multiphysics® 5.6 [46]. The effects of uncompensated ohmic resistance were quantified assuming one-dimensional semi-infinite linear diffusion, facile kinetics, and comparable diffusion coefficients for the oxidized and reduced species. Figure 14(a) shows the effect of increasing ohmic resistance contributions to simulated CVs on a 1 cm^2 electrode. Utilizing the anodic peak current from CVs with ideal and non-zero solution ohmic resistance, current multipliers (CM) were obtained as a function of varying observed peak broadening. CMs were extracted from simulated CVs using the following definition:[41]

$$\mathrm{CM} = \frac{I_\mathrm{p}(R_\Omega = 0)}{I_\mathrm{p}(R_\Omega > 0)} \quad [3]$$

In Figure 14(b), the calculated CMs were plotted as a function of $E_\mathrm{p}^\mathrm{a} - E_{\mathrm{p}/2}^\mathrm{a}$ at temperatures between 550 °C and 740 °C, two experimentally important temperatures. These CMs were then applied to the uncorrected peak current to yield a corrected current according to:

$$\Delta\, \mathrm{I_p^{corrected}} = \mathrm{CM} \times \Delta\, \mathrm{I_p^{uncorrected}} \quad [4]$$

To achieve accurate peak current density measurements, CMs were therefore applied to the anodic U^{3+}/U^{4+} peak for each electrode before the current output from the MAVS was converted to current density.

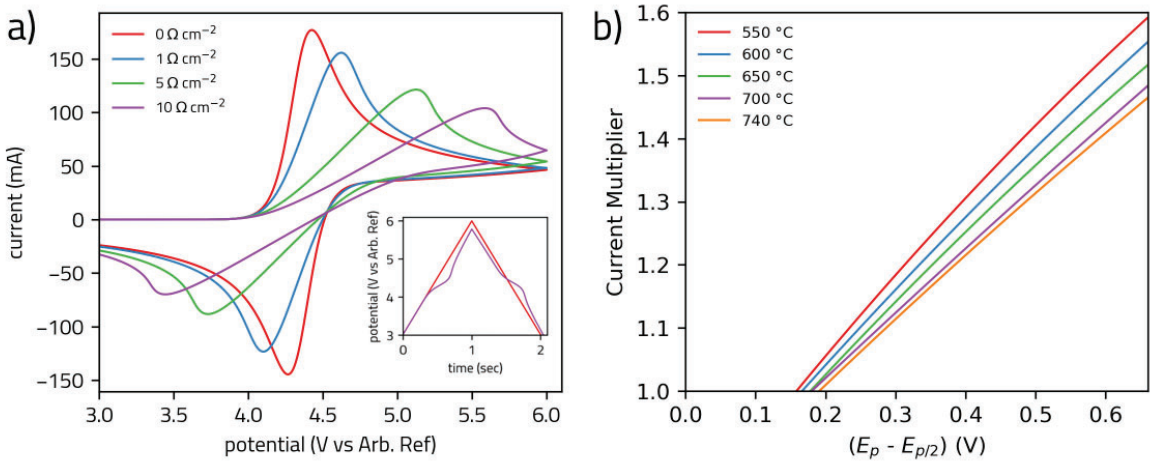

Figure 14. Results of COMSOL simulation (a) cyclic voltammograms with various amounts of uncompensated ohmic resistance and (b) current multiplier (CM) as a function of the difference between the anodic peak and half-peak potentials assuming a 1-electron transfer, soluble-soluble redox transition at 550 °C. The electrode surface area was 1 cm^2.

The use of current multipliers for the correction of data influenced by solution ohmic resistance was demonstrated by performing measurements with two electrochemical cell geometries which were susceptible to different R_Ω. Figure 15(a) depicts a typical set of voltammograms from each electrode in the MAVS in 6.7 mol/L UCl_3 for the geometry where δ equals 1 mm. For each set of measurements, the

electrode immersion depth was calculated by linear extrapolation of the anodic peak currents as a function of the known electrode stagger length (3 mm). Figure 15 (b) shows the peak current measurements as a function of the electrode immersion depth for the concentrations 6.7 mol/L and 4.1 mol/L. The data depicted in gray, which did not receive peak current corrections, demonstrated significant dependence on the cell geometry. However, after applying correction factors for ohmic resistance, the peak current and immersion depth (shown in color) were consistent regardless of the value of δ.

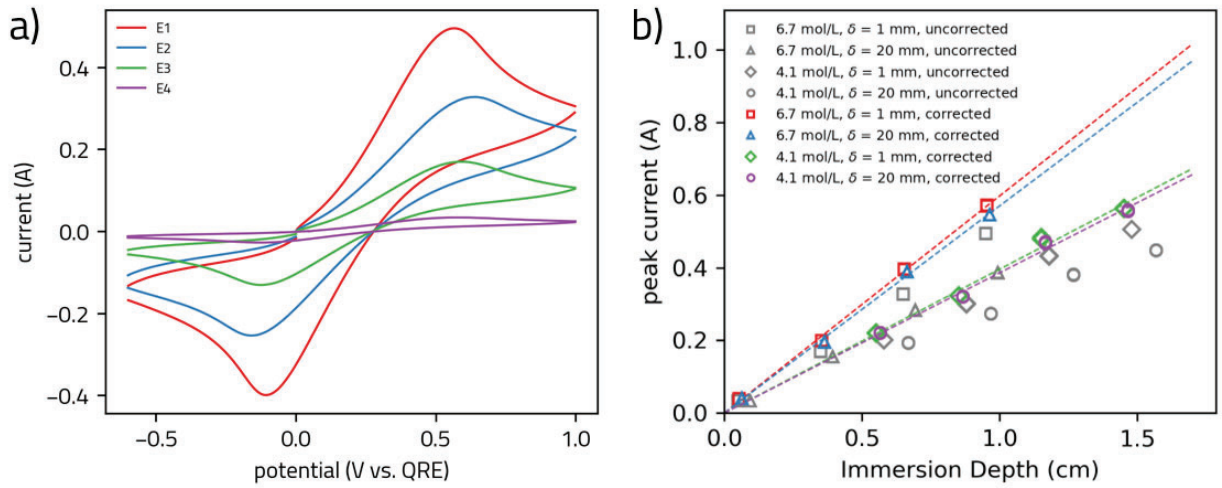

Figure 15. (a) Cyclic voltammograms of the U^{3+}/U^{4+} redox reaction in 6.68 mol/L U^{3+} using each electrode at 550 °C and (b) the anodic peak current as a function of the electrode immersion depth from two concentrations of U^{3+} and two electrochemical cell geometries. The initial potential scan direction is positive. The scan rate is 3000 mV s^{-1}.

For each concentration, measurements for each electrode were conducted in triplicate and a proportional linear fit to the three sets of data was applied as shown in Figure 15 (b). The slope of these linear fits was used to calculate the current density. The peak current density of the corrected data increased proportionally to the calculated concentration of U^{3+} from process knowledge, whereas the uncorrected data showed significant deviation. The U^{3+} diffusion coefficient was measured using the corrected peak current data at 3000 mV/sec and Equation 3. A representative diffusion coefficient for U^{3+} at these high concentrations at 550 °C of $4.1 \pm 0.4 \times 10^{-6}$ cm^2 s^{-1} was obtained by taking the average of values obtained from both cell geometries.

The U^{3+} concentration was calculated using the peak current densities and the average U^{3+} diffusion coefficient. Figure 16 shows a parity plot of U^{3+} concentration versus the known concentration from process knowledge for cases where the correction factor was and was not used. Without ohmic resistance corrections, the U^{3+} concentrations obtained from the two cell geometries did not agree, and there was significant deviation from the parity line. With ohmic resistance correction, the average error between the values obtained for each concentration from the two cell geometries was just 2.3%. The mean absolute relative error of all the corrected U^{3+} concentration measurements compared with known values was approximately 4.0%. The uncorrected values in turn had a mean absolute relative error of 20.4%. The results, as such, showed significant improvement in the precision and accuracy of the U^{3+} concentration measurement when the voltammetric data was properly corrected.

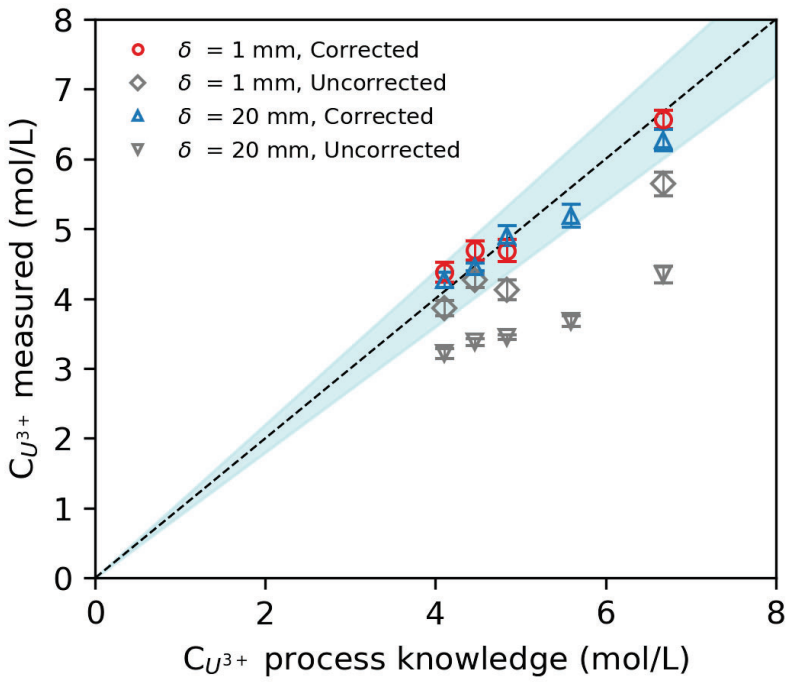

Figure 16. Parity plot comparing predicted U^{3+} concentration from voltammogram peak current density vs. the calculated concentration from process knowledge with and without ohmic resistance correction at 550 °C. Error bars represent the standard error in the electroanalytical measurement.

Several factors may influence the accuracy of the diffusion coefficient determination and thus the concentration predictions. The accuracy of the simulated current correction factor is based on key assumptions, including semi-infinite linear diffusion, facile kinetics, and comparable diffusion coefficients for the oxidized and reduced species. The presence of migration was also ignored, even though it may have an effect at these very high concentrations [21]. Furthermore, the accuracy of the calculated species concentration was dependent upon the validity of the salt density model at high concentrations of U^{3+}, and the rate of U^{3+} diffusion may depend on the acidity of the salt which influences complex formation in molten salts [47]–[48]. Nonetheless, even with these assumptions, the current multiplier approach as applied to very highly loaded salts enabled strong linear responses suitable for making quantitative measurements of species concentrations.

Although the correction factors generated from digital simulations were able to improve the concentration measurements considerably, the 4.0% mean absolute error was still larger than expected. Much of this error was a result of the fact that these experiments were the first time that the updated techniques had been attempted in ultra-high-concentration salts. Further improvements and iterations of the approaches, as described in Section 4, demonstrated that considerably lower error bounds (~1%) could eventually be achieved.

3. Salt Production Activities

Alongside producing salt for the flow systems, engineering-scale synthesis activities in FY25 offered the opportunity to test sensors in conditions relevant to front-end molten salt fuel fabrication. While several uranium chlorination reaction pathways have been demonstrated in the literature, few studies have proposed a method for near real-time analytical measurement of the concentration of uranium. Methods to verify salt composition and effective removal of the reaction byproducts are needed to optimize and safeguard the production process. As such, the electroanalytical approaches were applied to monitor and safeguard the chlorination of natural uranium during the synthesis of highly loaded LiCl-KCl-UCl_3 salts.

Chloride salts with high concentrations of UCl_3 have been produced from uranium metal by several reaction pathways. $PbCl_2$ [49], $CdCl_2$ [50], $CuCl_2$ [51], NH_4Cl [52], $ZrCl_4$ [53], and $FeCl_2$ [54] are viable chlorination reagents, but pose unique challenges that have been previously discussed [6]. Chlorination of depleted uranium metal by reacting it with $ZnCl_2$ in molten salt LiCl-KCl was shown by Lee et al. [55] and Rose et al. [56]. The exchange redox reaction between $ZnCl_2$ and U metal to form UCl_3 (1) has a negative Gibbs free energy of reaction.

$$3/2\,ZnCl_2 + U \rightarrow UCl_3 + 3/2\,Zn \;\; (\Delta G = -238.3\,kJ\;at\;500\,^{\circ}C) \qquad [5]$$

The formation of UCl_4 can be suppressed by contacting the salt with an excess of uranium metal [55]. The advantage of this reaction pathway is the volatilization of the resulting Zn metal can be regulated using the temperature. Thus, the reaction can be carried out and then the Zn product distilled to leave a pure salt with accurate composition.

Two experiments were successfully carried out to show efficient production of LiCl-KCl-UCl_3 salts with UCl_3 concentrations as high as 72.3 wt% at different scales. In both cases, efficient removal of the Zn reaction byproduct was demonstrated. The voltammetry sensors integrated into the production vessel were used throughout the process and showed good agreement with process knowledge and analytical chemistry results.

3.1. Bench-scale UCl_3 Salt Production and Monitoring

Bench-scale uranium chlorination experiments confirmed the efficacy of the $ZnCl_2$ uranium chlorination process and application of in situ voltammetry methodologies. LiCl-KCl-UCl_3 salts with varying concentrations of UCl_3 were synthesized by chlorinating natural uranium (NU) in 20 g of eutectic LiCl-KCl (58.2-41.8 mol%). Consecutive additions of $ZnCl_2$ were made to the salt and reacted with an excess of NU at 740 °C. Three salt compositions were synthesized with predicted compositions of 43.4, 57.9, and 72.3 wt% UCl_3. Figure 17 shows the salt containing 72.3 wt% UCl_3. The salt has a deep purple color that is consistent with similar salts reported [57] and is indicative of the presence of UCl_3.

Figure 17. LiCl-KCl-UCl_3 (72.3 wt% UCl_3) solidified in a boron nitride crucible.

Each salt was cooled, and a solid salt sample was taken for analytical chemistry measurements. Inductively coupled plasma-optical emission spectroscopy (ICP-OES) was used to measure the concentration of U and Zn after each chlorination. Table 2 shows the nominal composition of three salts produced for analysis and the results of ICP-OES analysis. The uncertainty of the reported ICP-OES results was 5%. The concentration of U measured by ICP-OES in mass fraction agreed well with process knowledge. Again, due to the wide compositional range investigated in this study, the ideal mixing density model [43] was used to approximate salt densities at 740 °C for conversion of analytical chemistry results to concentrations. The calculated molarity of UCl_3 in the salts that were investigated ranged from 2.7 mol/L to 6.3 mol/L, utilizing process knowledge value at 740 °C. Henceforth, the salt compositions are referred to by their calculated molarity based on process knowledge.

Table 2. Predicted LiCl-KCl-UCl_3 salt compositions and compositional data obtained from inductively coupled plasma optical emission spectroscopy.

U wt%	UCl_3 wt%	ρ_{calc} g/mL	M mol/L	U (ICP-OES) wt%	Zn (ICP-OES) wt%
30.0	43.4	2.1	2.7	30± 2	<0.04
40.0	57.9	2.5	4.2	40 ± 2	<0.04
50.0	72.3	3.0	6.3	51 ± 3	0.43 ± 04

Online salt composition data were obtained through voltammetry methods. Figure 18 shows cyclic voltammograms for eutectic LiCl-KCl following consecutive uranium chlorination steps. Reactions *a/a'*, *b/b'*, *c/c'*, and d' correspond to Li/Li^+, U/U^{3+}, U^{3+}/U^{4+}, and Cl^-/Cl_2, respectively. In salts containing greater than 2.7 mol/L UCl_3, reaction *b/b'* is the lower bound of the usable potential range. The peak current density of reaction *c/c'* increased with increasing UCl_3 concentration. As previously shown, the high currents and

finite ohmic resistance mean that voltammograms of reaction *c/c'* displayed significant peak broadening. The peak current of each voltammogram was corrected prior to analysis using the current multiplier for 740 °C shown in Figure 14(b). The U^{3+} diffusion coefficient was calculated by taking the average of the diffusion coefficients obtained using the slope of the proportional fit to the corrected peak current density in Figure 19(a) and Equation 3. Figure 19(b) shows triplicate measurements of the corrected anodic *c'* peak current plotted as a function of electrode surface area. The peak current density, as such, corresponded to the slope of the fit.

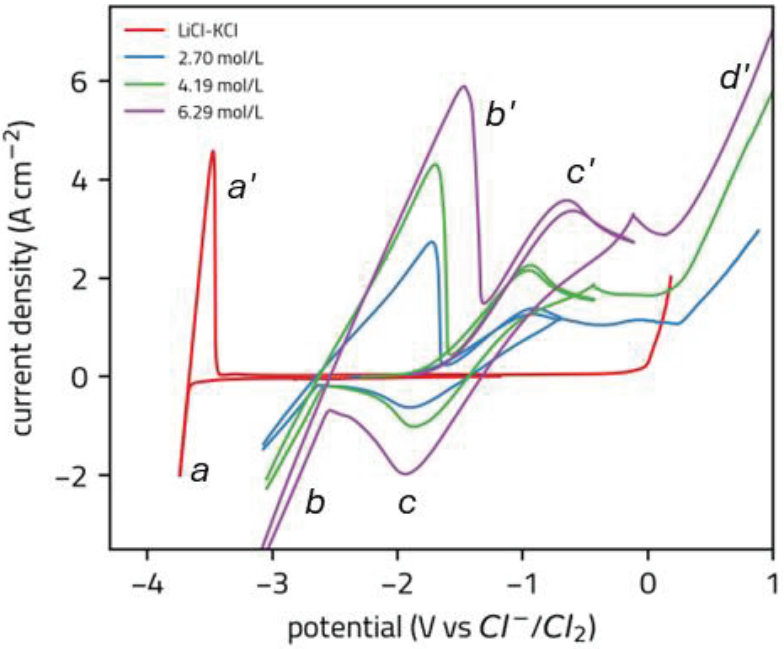

Figure 18. Cyclic voltammograms LiCl-KCl with various concentrations of UCl3 during the chlorination of natural uranium metal at 740 °C. The scan rate is 3000 mV/sec.

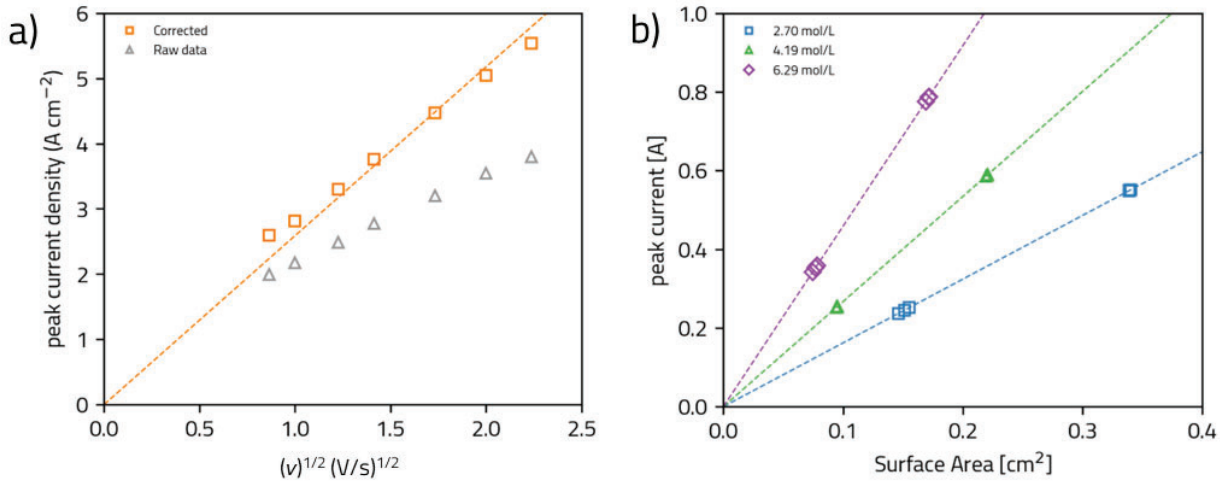

Figure 19. Voltammetric analysis of (a) U(III)/U(IV) oxidation peak current as a function of scan rate at 6.3 mol/L with correction for solution ohmic resistance, and (b) corrected U(III)/U(IV) oxidation peak current with respect to electrode surface area for various concentrations of UCl_3.

Species concentrations were calculated using the current density of peak *c'*, the corresponding diffusion coefficient, and Equation 3. Figure 20 shows a parity plot of the U^{3+} concentrations from voltammetry and process knowledge. The mean absolute relative error of the voltammetry measurements at 2.7, 4.2, and 6.3 mol/L was 7.9%. This relative error was likely inflated by inaccurate salt density data over the wide range of compositions tested. Improved diffusion coefficients can be generated by proper salt density measurements, but this was outside the scope of this project.

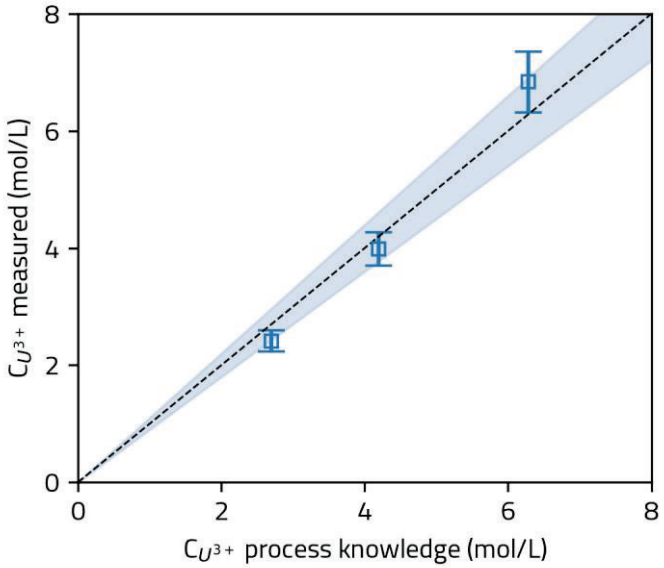

Figure 20. The concentration of UCl_3 in LiCl-KCl measured by voltammetry at 740 °C.

3.2. Engineering-scale UCl_3 Salt Production and Monitoring

To produce the salts needed for electrochemical sensor testing in high-concentration uranium molten salts, we designed and operated the engineering-scale UCl_3 production system shown in Figure 6. The salt, which was not commercially available in the weight loadings and compositions of interest, was needed to facilitate testing of a FEES using the Miniature-MFIT system shown in Figure 5. Figure 21 shows the natural uranium powder and the stainless-steel basket used to contact the metal with molten salt. Figure 22 depicts the 868 g of LiCl-KCl-UCl_3 (43.4 wt% UCl_3) produced during the first at-scale test batch. The synthesized salt had a deep purple color that was properly indicative of the presence of UCl_3.

Figure 21. Natural uranium powder precursor (left) and stainless steel mesh basket (right).

Figure 22. LiCl-KCl-UCl_3 (43.4 wt% UCl_3) salt produced by $ZnCl_2$ chlorination.

Voltammetric analysis of the 43.4 wt% UCl_3 salt was performed during the final stages of production in the engineering- scale UCl_3 production system. Figure 23 shows voltammograms across the usable potential range of the salt. Like previously results, the prominent redox reactions were (*b/b'*) U/U(III), (*c/c'*) U(III)/U(IV), and (*d'*) evolution of chlorine gas. No redox peaks corresponding to the Zn/Zn(II) reaction were present, indicating effective removal of the reaction byproduct. Characterization of the synthesized salt is underway using inductively coupled plasma optical spectroscopy and differential scanning calorimetry.

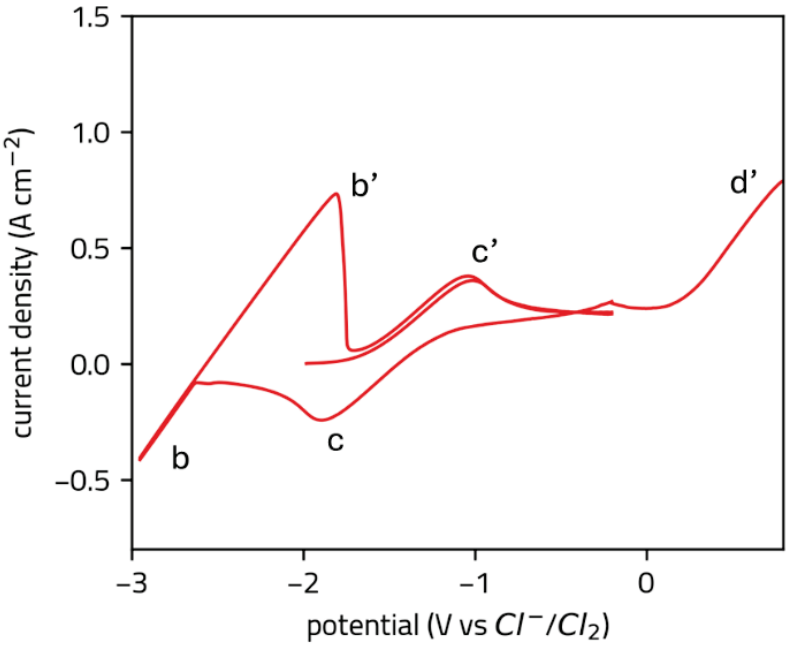

Figure 23. Cyclic voltammograms of LiCl-KCl-UCl_3 (43.4 wt% UCl_3) at 610 °C. The scan rate is 3000 mV/sec.

4. FY25 Assessment of Electrochemical Sensor Performance in Complex High-Concentration Actinide Salts

4.1. Assessment of FEES Performance in High-Concentration Actinide Salts

Flow enhanced electrochemical sensor measurements were conducted in LiCl-KCl-UCl_3 (43.4 wt% UCl_3) to assess the precision of actinide measurements in salts with very high actinide concentrations. Flow tests were conducted in a Miniature-MFIT in a radiological glovebox using 668 g of natural uranium-bearing salt (30 wt% U). The Miniature-MFIT approach allowed for the use of relatively small quantities of radiological materials and enabled FEES measurements in carefully controlled flowing salt conditions. Measurements were carried out at flow rates between 0.1 and 0.8 L min^{-1}.

The operating principles of the FEES sensor were relatively straightforward compared to voltammetry sensors, provided there is adequate knowledge of the oxidation potential of the species of interest. Prior to constant potential measurements, the FEES sensor was operated as a typical voltammetry probe to ascertain the appropriate constant potential value for the chronoamperometric UCl_3 measurements. Figure 24(a) shows a voltammogram of the salt at 0.3 L min^{-1}. Reactions *c'* and d' correspond to the oxidation of U^{3+} to U^{4+} and the evolution of Cl_2 gas, respectively. To achieve repeatable FEES sensor measurements, an appropriate constant potential value positive of peak *c'* was applied. Care must be taken not to evolve Cl_2 gas during the measurement to ensure accuracy and longevity of the sensor. Figure 24 depicts constant potential FEES measurements at various flow rates. The sensor's current response was similar to measurements taken previously in low concentration salts. The response included characteristics of (1) an initial startup period, (2) a subsequent current plateau during constant flow, and (3) a decrease in current as the salt is allowed to drain out of the MFIT. As expected, the magnitude of the current plateau increased with flow rate.

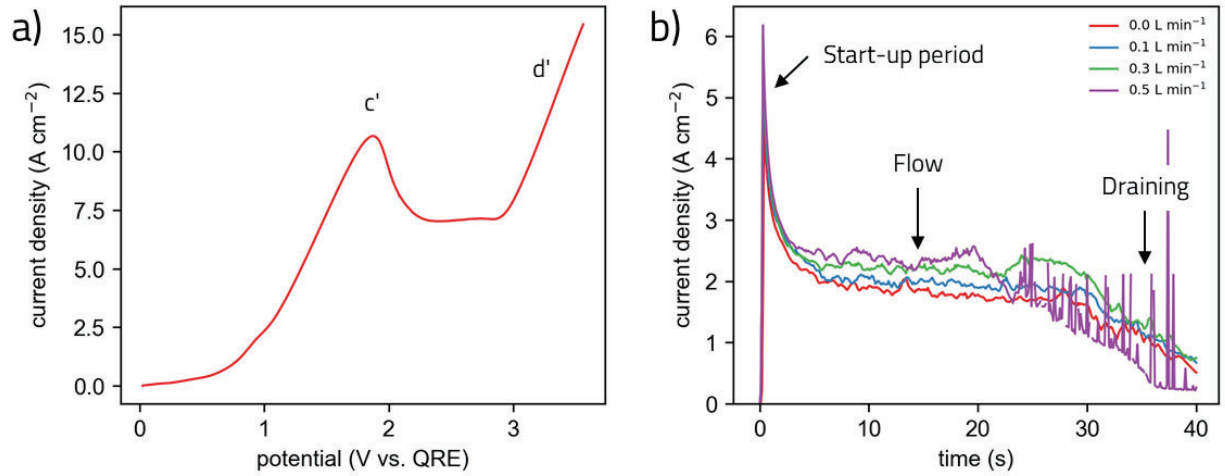

Figure 24. Flow-enhanced electrochemical sensor (a) voltammogram depicting the oxidation potential of species relative to the quasi-reference electrode and (b) the constant potential current output in flowing LiCl-KCl-UCl_3.

Analysis of the FEES measurements involved taking the average of the current density after the startup period, when the sensor experienced constant flow. Typically, the measurements were started 5 to 10 seconds after applying the constant potential. Measurements of the 43.4 wt% UCl_3 salt were recorded in quadruplicates at flow rates between 0.1 L min^{-1} and 0.8 L min^{-1}. The average current response at each flow rate is shown in Figure 25. Typical current densities encountered over this range of flow rates were almost a magnitude higher than measurements conducted in 3 wt% UCl_3 at higher flow rates (3 to 7 L min^{-1}) [6], showing the strong effect of highly concentrated analytes. Despite the high currents, the signal-to-noise

ratio was good, and the average standard deviation of measurements taken at each concentration was 1.3%. Random errors of around 1% are consistent with the results taken at low UCl_3 concentrations in previous years.

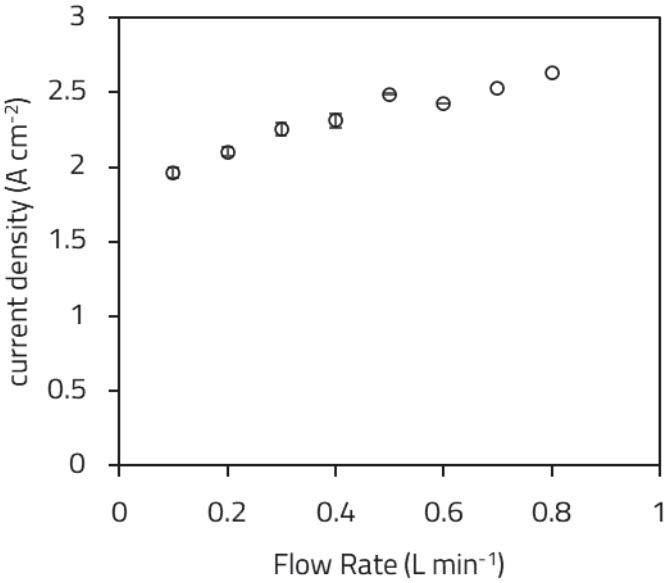

Figure 25. FEES sensor current response to in LiCl-KCl-UCl_3 (43.4 wt% UCl_3) with respect to flow rate.

4.2. Voltammetry Measurements of Highly Loaded UCl_3-Bearing Fuel Salts in the Presence of Surrogate Fission Products

As a final test of voltammetry techniques for highly loaded salts, stationary measurements of UCl_3-bearing salts containing dissolved fission products were performed. Liquid fuel MSRs are characterized by both a large fissile inventory and transient quantities of SNM due to transmutation and depletion. To maintain material balance, accurate and selective sensors for species of interest are required. Nuclear fission of uranium will result in some products that are soluble in molten salt and thus could affect the uranium concentration determination. The fission products Rb, Sr, Y, Zr, Ba, La, Ce and other rare earths have been shown to be stable and soluble in molten fluoride salts. Other noble-metal fission products (Nb, Mo, Tc, Tc, Ru, Pd and I) may not form chlorides that are thermodynamically stable in the salt and may leave the system as gases or plate out on vessel walls [58]. These fission products are expected to be a concern for molten chloride salt fast reactors [59]–[60]. Voltammetry sensors can be selective for specific soluble species, provided that the thermodynamic reaction potentials of each species are sufficiently different. In this study, the selectivity of the voltammetry sensor for uranium is demonstrated in the presence of a variety of dilute fission product surrogates.

To identify fission products of interest, a survey was conducted of species that could complicate uranium chloride voltammetry measurements because they form long-lived and soluble chlorides in the melt. Table 3 shows fission products capable of forming stable chlorides and their half-lives. Comparison of the chloride calculated standard reduction potentials enables assessment of the challenge they pose to voltammetry measurements. Species with oxidation potentials lower than UCl_3 are less likely to generate current responses that are convoluted with current corresponding to the oxidation of U^{3+} to U^{4+} during the anodic voltammetry sweep. Table 3 shows that few soluble species have oxidation potentials higher than the U^{3+} to U^{4+} reaction. Therefore, the soluble fission products are unlikely to pose issues for voltammetry measurements of the oxidation reaction of U^{3+} to U^{4+}.

Table 3. Soluble fission product half-life and standard reduction potential calculated using HSC **[61]**.

Isotope	Electrochemical Redox Reaction	Half-life	Stability	Standard Reduction potential at 550 °C (V)
^{143}Pr	$Pr^{4+} + e^- \rightarrow Pr^{3+}$			5.013
^{148}Nd	$Nd^{4+} + e^- \rightarrow Nd^{3+}$			6.230
^{147}Sm	$Sm^{4+} + e^- \rightarrow Sm^{3+}$			6.505
$^{141}Ce/^{144}Ce$	$Ce^{4+} + e^- \rightarrow Ce^{3+}$			3.133
^{235}U	$U^{4+} + e^- \rightarrow U^{3+}$			0.892
^{235}U	$U^{3+} + 3e^- \rightarrow U^0$			-1.155
^{143}Pr	$Pr^{3+} + 3e^- \rightarrow Pr^0$	13.57 days	Soluble	-1.781
^{147}Sm	$Sm^{3+} + 3e^- \rightarrow Sm^0$	Stable	Soluble	-1.781
^{91}Y	$Y^{3+} + 3e^- \rightarrow Y^0$	59 days	Soluble	-1.756
^{148}Nd	$Nd^{3+} + 3e^- \rightarrow Nd^0$	11.1 days	Soluble	-1.811
^{140}La	$La^{3+} + 3e^- \rightarrow La^0$	40.3 hours	Soluble	-1.848
^{141}Ce	$Ce^{3+} + 3e^- \rightarrow Ce^0$	32.3 days	Soluble	-1.844
^{144}Ce		284 days	Soluble	
^{140}Ba	$Ba^{2+} + 2e^- \rightarrow Ba^0$	12.8 days	Soluble	-2.807
^{89}Sr	$Sr^{2+} + 2e^- \rightarrow Sr^0$	52 days	Soluble	-2.720
^{90}Sr		28.1 years	Soluble	
^{91}Sr		9.67 hours	Soluble	
^{133}Cs	$Cs^+ + e^- \rightarrow Cs^0$	Stable	Soluble	-3.808
^{134}Cs		705 days	Soluble	
^{137}Cs		29.9 years	Soluble	

To confirm the selectivity of the voltammetric UCl_3 measurements, soluble fission products surrogates were sequentially added to a LiCl–KCl–UCl_3 melt containing 50 wt% U (≈72.3 wt% UCl_3). To approximate upper-bound concentrations expected during extended high-burnup MSR operations [4], $CeCl_3$, $LaCl_3$, and $NdCl_3$ were first added in quantities equal to 1 wt% each, representing ~30 years of operation. Additional rare earth surrogates ($SmCl_3$, $PrCl_3$, YCl_3) were next added at ~1 wt% each to broadly represent other lanthanides that may be present. Finally, to probe the effect of chloride stoichiometry, dichlorides ($BaCl_2$, $SrCl_2$) and a monochloride (CsCl) were then also added to confirm that variations in chloride coordination do not influence the voltammetric detection of uranium. After the three additions consisting of three species each, voltammetry was performed to monitor the U^{3+}/U^{4+} redox couple ($U^{3+} \rightarrow U^{4+} + e^-$). As shown in Figure 26, the anodic peaks associated with U^{3+} oxidation (labeled *c'*) remained unchanged in potential and shape, indicating that the additives did not interfere with voltammetric quantification of UCl_3 under the conditions tested.

Quantification of the uranium concentration throughout these additions showed excellent agreement with process knowledge. Figure 27 shows the stepwise change in U concentration after each surrogate addition, along with the corresponding values measured by voltammetry. As is evident, the measured uranium concentrations closely matched the values expected during the progressive dilution of the original salt.

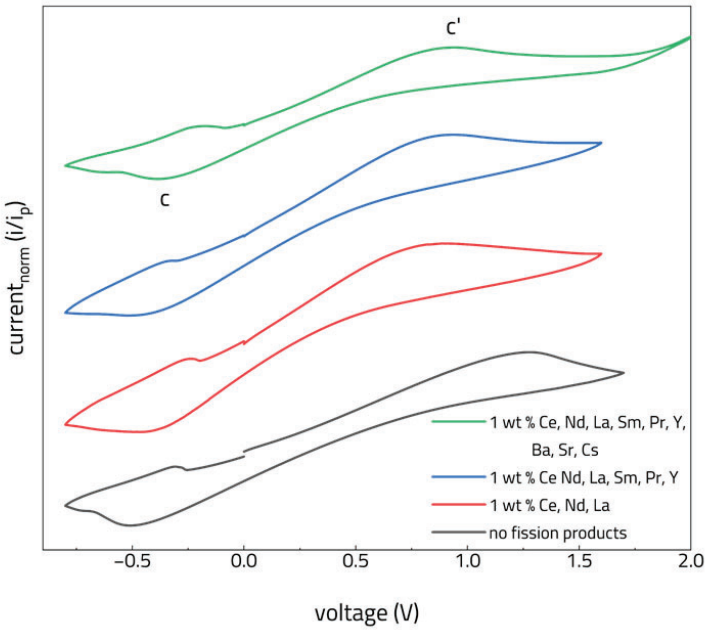

Figure 26. Cyclic voltammograms of LiCl-KCl-UCl_3 (6.7 x 10^{-3} mol/cm^3 UCl_3) with various additions of fission product surrogates.

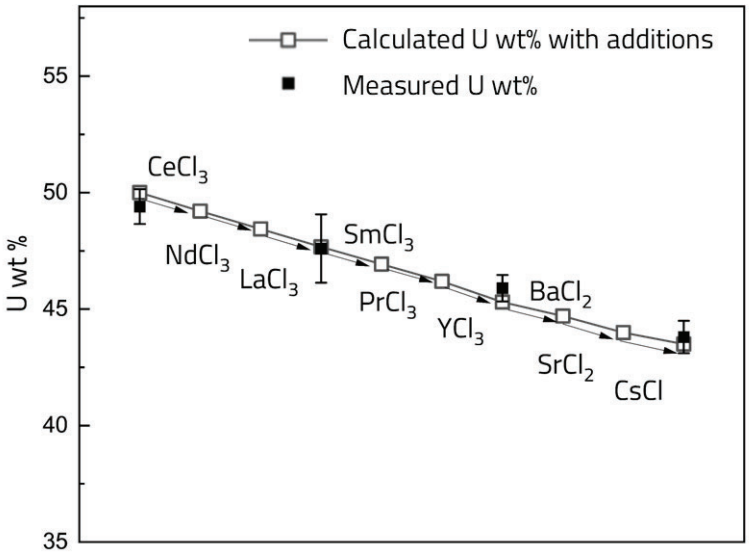

Figure 27. Measured and calculated concentrations of U in LiCl-KCl-UCl_3 with sequential additions of surrogate fission products.

Parity plots of the known and measured uranium concentrations also demonstrated excellent agreement, as shown in Figure 28. Over the entire course of the additions, the voltammetrically measured concentrations demonstrated a mean absolute relative error of only 0.8%. This error level was superior to what had been

achieved during initial tests of the high-concentration voltammetry techniques due to improvements in sensor robustness and electrode calibration.

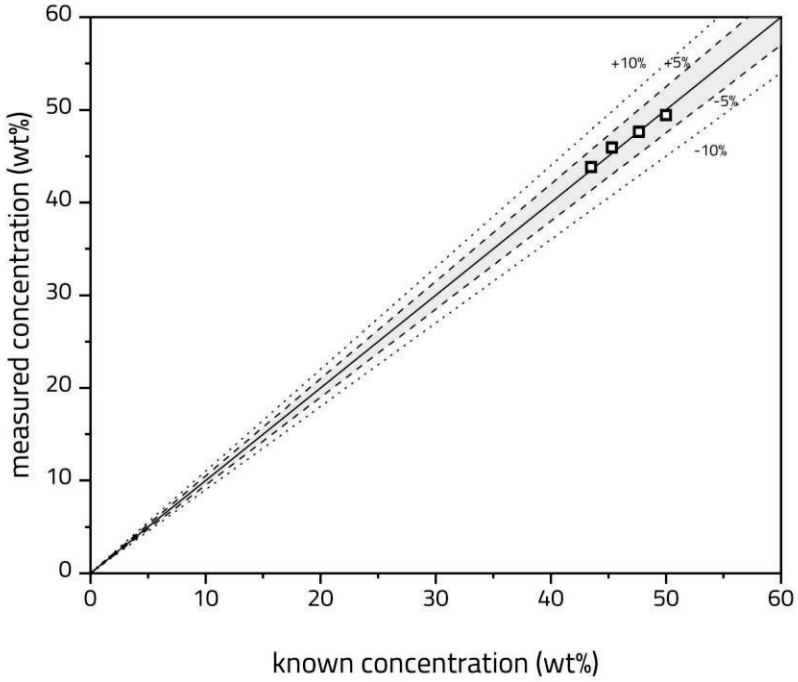

Figure 28. Parity plot showing measured and known uranium concentrations during additions of fission product surrogates

5. Sensor Deployments to Industrial Partner Facilities

As part of ARSS, Argonne National Laboratory partnered with two MSR vendors to test deployed sensors at their facilities. In FY24, FEES sensors were tested at Kairos Power, LLC in a FLiBe salt test loop. In FY25, voltammetry sensors were deployed to TerraPower, LLC for evaluation in chloride salts. These sensor deployments are excellent opportunities to advance sensor technical readiness level in challenging real-world environments.

5.1. Flow enhanced electrochemical sensors at Kairos Power, LLC FLiBe salt test loop

Argonne National Laboratory deployed an advanced electrochemical system to Kairos Power's salt test loop in FY24 [6]. The loop, shown in Figure 29(a), is a forced convection flow system containing 15 kg of FLiBe LiF-BeF_2 (66:34 mol %) salt. This activity enabled in-line flow-enhanced electrochemical sensors, shown in Figure 29(b) evaluation in a flowing non-radiological environment. The sensors were carefully sealed to enable them to operate fully submerged. To enable these tests, Argonne has developed a novel electrochemical control system and ILEX Automation© software, shown in Figure 29(c), which could remotely control up to twelve electrochemical cells in the Kairos test loop.

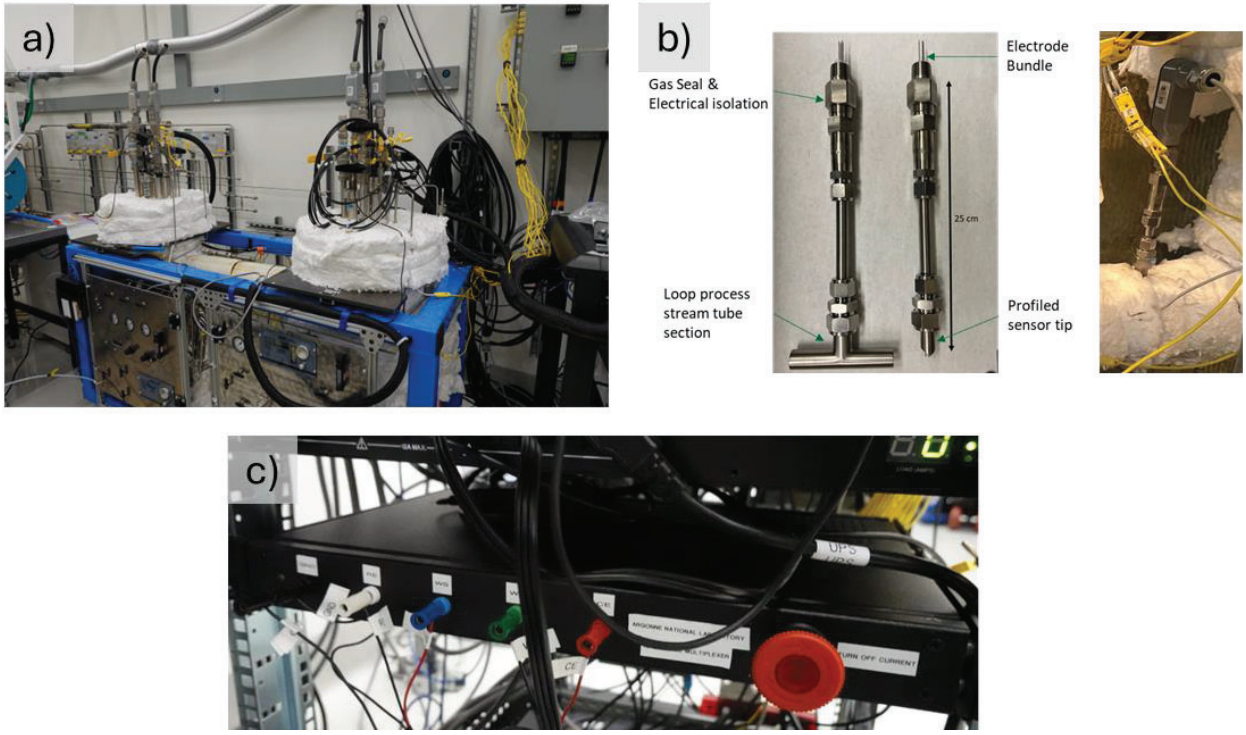

Figure 29. (a) Kairos Power's FLiBe salt test loop, (b) in-line flow-enhanced electrochemical sensors and (c) a custom 12-channel multiplexer for controlling electrochemical sensors [6].

The flow-enhanced electrochemical sensors monitored the composition of the FLiBe salt and the structural health of the salt test loop. Figure 30, shows an example of a typical voltammogram obtained from the sensors during loop operations. To protect specific details regarding the operation of the loop, the potential axis and other information have been omitted. The sensors endured over 900 hours of loop operations without noticeable damage or leaks. Electrochemical monitoring ultimately provided key insights into the long-term operations of Kairos' molten salt equipment.

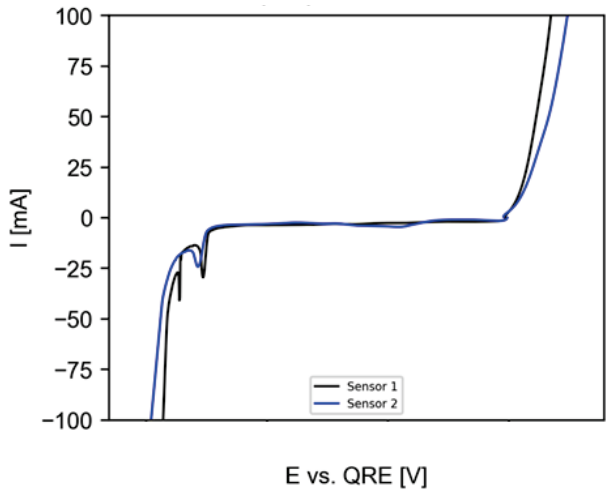

Figure 30. In-line electrochemical sensor voltammetry measurements of circulating FLiBe salt in the Kairos test loop.

5.2. Sensor benchmarking in stationary NaCl-$MgCl_2$-$CrCl_2$ at TerraPower

In FY25, Argonne National Laboratory deployed a voltammetry sensor to TerraPower LLC for evaluation in chloride salts relevant to the Molten Chloride Fast Reactor (MCFR). The objective of this research was to demonstrate online salt chemistry monitoring in non-radiological NaCl-$MgCl_2$ to form the technical basis for deployment in TerraPower's radiological systems. In this research, the redox behavior of simulated $CrCl_2$ corrosion product was investigated over a range of concentrations and temperatures. The result was a set of parameters that could be used to calculate Cr^{2+} concentration in this molten salt system.

The multielectrode array voltammetry sensor was tested in bench-scale stationary salt systems inside of a glovebox at TerraPower shown in Figure 31. Argonne National Laboratory deployed both an industrialized multielectrode array voltammetry sensor (MAVS) and a multiplexer control system. The sensor was remotely operated by researchers at Argonne using ILEX Automation© software.

Figure 31. Stationary molten salt system at TerraPower LLC.

In coordination with TerraPower staff, measurements were taken in NaCl-$MgCl_2$ with various concentrations of $CrCl_2$ and at different temperatures. A typical voltammogram obtained in this salt is shown in Figure 32(a). The axes have been removed to protect operational conditions associated with this specific salt system. Chromium chloride showed one set of clear redox peaks at all concentrations and temperatures investigated, corresponding to the redox reaction Cr^0/Cr^{2+}. This enabled straightforward single-species concentration measurements. Although alternate electroanalytical approaches could also be used in this system, linear sweep voltammetry was selected as the resulting signals can be readily analyzed to address non-idealities encountered in large-scale systems [5].

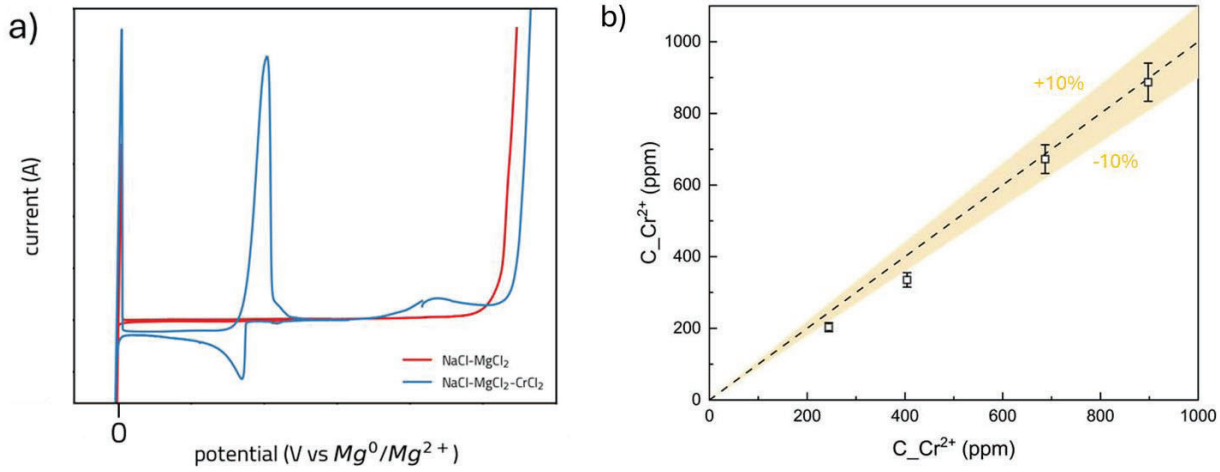

Figure 32. Voltammograms of (a) NaCl-$MgCl_2$ with and without additions of $CrCl_2$ and (b) measurements of Cr concentration in NaCl-MgCl2 with process knowledge concentration of Cr at 590 °C.

To facilitate species concentration measurements over a range of test conditions, diffusion coefficients for $CrCl_2$ were obtained. Figure 32 (b) depicts measurements that were made over a range of temperatures and concentrations based on process knowledge. A definitive analysis of these measurements is planned, but is pending the results of ICP-OES to confirm the salt composition. The plot axes have again been intentionally removed to protect intellectual property associated with the industrially relevant salt and its expected operational conditions. Using the process knowledge, the results showed a preliminary mean absolute relative error of 9% for Cr^{2+} concentration measurements over the range of concentrations studied. Updated information, such as offline analyses will likely improve these results. Argonne National Laboratory will continue to coordinate with TerraPower LLC regarding potential sensor deployments in natural circulation loops in FY26.

6. Sensor Performance Assessment

The FEES and MAVS electrochemical sensor technologies under development for ARSS have displayed good capabilities for measuring actinide concentrations in realistic salt mixtures throughout the past five years. New techniques and approaches were developed throughout that time that led to discrete improvements in capabilities. These new capabilities were often accompanied by temporary increases in systematic errors associated with the measurements, but the uncertainties were eventually able to be reduced as additional time, developmental effort, and honing of the new techniques occurred. For example, as of FY24, systematic uncertainty for measurements of high-concentration uranium in fuel salt mixtures was around 4%. Much lower uncertainties were eventually able to be achieved in FY25 when the systematic errors were reduced to only 0.8%. Table 4 shows the final systematic and random uncertainty components for these measurements after the culmination of the project activities. The values are very good for in-situ monitoring techniques and compare well to internationally-deployed systems [62].

Table 4. Performance of FEES/Electrochemical Sensors for High-Concentration Fuel Salts.

Measurement	Monitoring Tool	Uncertainty Component (%rel.)	
		Systematic Error	Random Error
Uranium Concentration in Highly Concentrated Fuel Salts (>30 wt% U)	FEES/Electrochemical Sensors	0.8%	1.3%

Complications from in-line and on-line monitoring operations within a full-scale MSR could lead to increased real-world uncertainties compared to these values, but the testing platforms developed at Argonne were designed to capture as many sources of non-idealities as possible. Nonetheless, it is expected that the errors for sensors operating in an MSR could be as high as 2× the values reported here. A full assessment of these uncertainties, however, will not be possible until these monitoring tools are able to be installed into an actual reactor. The feasibility of using these sensors for MC&A purposes is also unclear. While the uncertainty values of the in-situ measurements are very low, the large quantity of fissile material in an MSR at any time could cause the standard error of the inventory difference (SEID) to exceed the requirements listed in 10 CFR 74. Alternate approaches to safeguards, including anomaly-detection-based schemes or the use of sensor fusion capabilities to improve uncertainty levels, could help to resolve these issues, but more investigation must be done.

7. Conclusions

In FY25 significant progress towards development of flow enhanced electrochemical sensors and voltammetry techniques for MC&A of complex high concentration molten salts was made including (1) the application of new voltammetry techniques for accurate measurements of highly concentrated actinide salts, (2) the application of sensors to fuel fabrication and flow systems, and (3) sensor demonstrations in challenging real-world conditions at partner MSR institutions. Utilizing new voltammetry simulation tools, accurate measurements of UCl_3 concentrations in salts with mass fractions up to 72.3% were achieved. FEES were tested in salts with concentrations up to 43.4 wt% UCl_3 and were found to have similar performance to earlier tests conducted at much lower concentrations. Finally, the voltammetric approaches for measuring uranium chloride concentrations were shown to be independent of the concentration of multiple relevant fission products, including Ce, Nd, La, Sm, Pr, Y, Ba, Sr, Cs, and Zn.

Argonne National Laboratory also successfully demonstrated electroanalytical tools in relevant testing environments located at MSR partner vendors. In FY24, two FEES sensors were operated for over 900 hours in a FLiBe salt test loop at Kairos Power, LLC. In FY25, MAVS sensors were tested in stationary chloride salts containing simulated $CrCl_2$ corrosion products at TerraPower, LLC.

In total, the work conducted over the past five years for the ARSS program has served to enable the development of new safeguards-relevant monitoring tools along with the creation of several testing platforms that supported sensor assessments in real-world conditions. The capabilities for automated operations that were developed also permitted complex combined flow scenarios with synchronized sensor operations. The combined activities and technologies developed therein have substantially improved domestic capabilities for achieving MC&A and safeguarding of special nuclear material (SNM) in molten salt systems.

References

[1] K. K. Hogue, N. Luciano, M. Krupcale, R. Elzohery, and L. G. Evans, "Planning for Material Control and Accountancy at Liquid Fueled Molten Salt Reactors," Oak Ridge National Laboratory (ORNL), Oak Ridge, TN (United States), ORNL/SPR-2023/3181, Jan. 2024. doi: 10.2172/2283859.

[2] N. Shoman and M. Higgins, "Material Accountancy for Molten Salt Reactors: Challenges and Opportunities," Sandia National Laboratories, SAND2023-01845R, Apr. 2023. [Online]. Available: https://www.sandia.gov/app/uploads/sites/273/2024/01/Material-Accountancy-for-Molten-Salt-Reactors-Challenges-and-Opportunities.pdf

[3] N. C. Hoyt, M. A. Williamson, and J. L. Willit, "Multielectrode sensor for concentration and depth measurements in molten salt," Argonne National Laboratory (ANL), Argonne, IL (United States), 10,955,375, Mar. 2021. Accessed: Jan. 28, 2024. [Online]. Available: https://www.osti.gov/biblio/1805658

[4] J. Guo, N. Hoyt, and M. Williamson, "Multielectrode array sensors to enable long-duration corrosion monitoring and control of concentrating solar power systems," *J. Electroanal. Chem.*, vol. 884, p. 115064, Mar. 2021, doi: 10.1016/j.jelechem.2021.115064.

[5] N. C. Hoyt, J. L. Willit, and M. A. Williamson, "Communication—Quantitative Voltammetric Analysis of High Concentration Actinides in Molten Salts," *J. Electrochem. Soc.*, vol. 164, no. 2, p. H134, Jan. 2017, doi: 10.1149/2.1481702jes.

[6] W. Doniger, M. Jubinsky, C. Moore, N. Shaheen, and N. Hoyt, "Assessment of Flow-Enhanced Electrochemical Sensor Testing and Deployments," Argonne National Laboratory, ANL/CFCT-24/29, Sep. 2024.

[7] S. D. Branch *et al.*, "Optical techniques for advanced salt systems," Pacific Northwest National Laboratory, PNNL-36705, Sep. 2024.

[8] A. Sagadevan *et al.*, "Experimental Validation of Nondestructive Assay Capabilities for Molten Salt Reactor Safeguards," Los Alamos National Lab, ORNL/TM-2021/2288, Sep. 2021.

[9] E. Lukosi, "Microfluidic Alpha Spectrometry of UOX PWR UNF in a Molten Salt," *Nucl. Sci. Eng.*, vol. 188, no. 3, pp. 294–302, Dec. 2017, doi: 10.1080/00295639.2017.1367248.

[10] D. S. Poa, Z. Tomczuk, and R. K. Steunenberg, "Voltammetry of Uranium and Plutonium in Molten LiCl-NaCl-$CaCl_2$-$BaCl_2$: I . Reduction of U(III) to Uranium Metal1," *J. Electrochem. Soc.*, vol. 135, no. 5, p. 1161, May 1988, doi: 10.1149/1.2095904.

[11] K. Serrano and P. Taxil, "Electrochemical reduction of trivalent uranium ions in molten chlorides," *J. Appl. Electrochem.*, vol. 29, no. 4, pp. 497–503, Apr. 1999, doi: 10.1023/A:1003402029895.

[12] B. Prabhakara Reddy, S. Vandarkuzhali, T. Subramanian, and P. Venkatesh, "Electrochemical studies on the redox mechanism of uranium chloride in molten LiCl–KCl eutectic," *Electrochimica Acta*, vol. 49, no. 15, pp. 2471–2478, Jun. 2004, doi: 10.1016/j.electacta.2004.02.002.

[13] P. Masset *et al.*, "Electrochemistry of Uranium in Molten LiCl-KCl Eutectic," *J. Electrochem. Soc.*, vol. 152, no. 6, pp. A1109–A1115, Jun. 2005, doi: 10.1149/1.1901083.

[14] S. A. Kuznetsov, H. Hayashi, K. Minato, and M. Gaune-Escard, "Electrochemical Behavior and Some Thermodynamic Properties of UCl_4 and UCl_3 Dissolved in a LiCl-KCl Eutectic Melt," *J. Electrochem. Soc.*, vol. 152, no. 4, p. C203, Mar. 2005, doi: 10.1149/1.1864532.

[15] S. A. Kuznetsov, H. Hayashi, K. Minato, and M. Gaune-Escard, "Electrochemical transient techniques for determination of uranium and rare-earth metal separation coefficients in molten salts," *Electrochimica Acta*, vol. 51, no. 12, pp. 2463–2470, Feb. 2006, doi: 10.1016/j.electacta.2005.07.028.

[16] R. O. Hoover, M. R. Shaltry, S. Martin, K. Sridharan, and S. Phongikaroon, "Electrochemical studies and analysis of 1–10 wt% UCl_3 concentrations in molten LiCl–KCl eutectic," *J. Nucl. Mater.*, vol. 452, no. 1, pp. 389–396, Sep. 2014, doi: 10.1016/j.jnucmat.2014.05.057.

[17] M. M. Tylka, J. L. Willit, J. Prakash, and M. A. Williamson, "Method development for quantitative analysis of actinides in molten salts," *J. Electrochem. Soc.*, vol. 162, no. 9, pp. H625–H633, 2015, doi: 10.1149/2.0401509jes.

[18] M. M. Tylka, J. Willit, J. Prakash, and M. A. Williamson, "Application of Voltammetry for Quantitative Analysis of Actinides in Molten Salts," *J. Electrochem. Soc.*, vol. 162, no. 12, pp. H852–H859, 2015, doi: 10.1149/2.0281512jes.

[19] D. S. Maltsev, V. A. Volkovich, B. D. Vasin, and E. N. Vladykin, "An electrochemical study of uranium behaviour in LiCl–KCl–CsCl eutectic melt," *J. Nucl. Mater.*, vol. 467, pp. 956–963, Dec. 2015, doi: 10.1016/j.jnucmat.2015.10.014.

[20] N. C. Hoyt, J. L. Willit, and M. A. Williamson, "Communication—Quantitative Voltammetric Analysis of High Concentration Actinides in Molten Salts," *J. Electrochem. Soc.*, vol. 164, no. 2, p. H134, Jan. 2017, doi: 10.1149/2.1481702jes.

[21] D. Rappleye, K. Teaford, and M. F. Simpson, "Investigation of the effects of uranium(III)-chloride concentration on voltammetry in molten LiCl-KCl eutectic with a glass sealed tungsten electrode," *Electrochimica Acta*, vol. 219, no. Supplement C, p. 231, Nov. 2016, doi: 10.1016/j.electacta.2016.10.075.

[22] S. R. Pouri and S. and Phongikaroon, "An Interactive Reverse-Engineering Cyclic Voltammetry for Uranium Electrochemical Studies in LiCl-KCl Eutectic Salt," *Nucl. Technol.*, vol. 197, no. 3, pp. 308–319, Mar. 2017, doi: 10.1080/00295450.2016.1273730.

[23] D. Yoon and S. Phongikaroon, "Measurement and Analysis of Exchange Current Density for U/U3^{+} Reaction in LiCl-KCl Eutectic Salt via Various Electrochemical Techniques," *Electrochimica Acta*, vol. 227, pp. 170–179, Feb. 2017, doi: 10.1016/j.electacta.2017.01.011.

[24] K. Liu *et al.*, "The Application of Low-Melting LiCl-KCl-CsCl Eutectic to Electrodeposit Uranium Metal," *J. Electrochem. Soc.*, vol. 166, no. 13, p. D606, Aug. 2019, doi: 10.1149/2.0451913jes.

[25] S. Geran, P. Chamelot, J. Serp, M. Gibilaro, and L. Massot, "Electrochemistry of uranium in molten LiCl-LiF," *Electrochimica Acta*, vol. 355, p. 136784, Sep. 2020, doi: 10.1016/j.electacta.2020.136784.

[26] C.-Y. Jung, T.-H. Kim, and S.-E. Bae, "Real-time monitoring of uranium concentration in NaCl–$MgCl_2$–UCl_3 molten salt," *J. Radioanal. Nucl. Chem.*, vol. 332, no. 12, pp. 5233–5238, Dec. 2023, doi: 10.1007/s10967-023-09000-5.

[27] F. Fang *et al.*, "The Electrode Kinetics of UCl_3 in LiCl-KCl Molten Salt," *J. Electrochem. Soc.*, vol. 171, no. 5, p. 056504, May 2024, doi: 10.1149/1945-7111/ad4683.

[28] C. Hamel, P. Chamelot, A. Laplace, E. Walle, O. Dugne, and P. Taxil, "Reduction process of uranium(IV) and uranium(III) in molten fluorides," *Electrochimica Acta*, vol. 52, no. 12, pp. 3995–4003, Mar. 2007, doi: 10.1016/j.electacta.2006.11.018.

[29] M. Straka, M. Korenko, and F. Lisý, "Electrochemistry of uranium in LiF–BeF_2 melt," *J. Radioanal. Nucl. Chem.*, vol. 284, no. 1, pp. 245–252, Apr. 2010, doi: 10.1007/s10967-010-0478-8.

[30] C. Nourry, P. Souček, L. Massot, R. Malmbeck, P. Chamelot, and J.-P. Glatz, "Electrochemistry of uranium in molten LiF–CaF_2," *J. Nucl. Mater.*, vol. 430, no. 1, pp. 58–63, Nov. 2012, doi: 10.1016/j.jnucmat.2012.06.028.

[31] M. Korenko, M. Straka, L. Szatmáry, M. Ambrová, and J. Uhlíř, "Electrochemical separation of uranium in the molten system LiF–NaF–KF–UF_4," *J. Nucl. Mater.*, vol. 440, pp. 332–337, Sep. 2013, doi: 10.1016/j.jnucmat.2013.04.078.

[32] H. Peng, M. Shen, Y. Zuo, X. Tang, R. Tang, and L. Xie, "Electrochemical technique for detecting the formation of uranium-containing precipitates in molten fluorides," *Electrochimica Acta*, vol. 222, pp. 1528–1537, 2016, doi: 10.1016/j.electacta.2016.11.135.

[33] F. Jiang *et al.*, "Electrochemical behavior and electrowinning of uranium(IV) from FLiNaK molten salt," *J. Radioanal. Nucl. Chem.*, vol. 311, no. 3, pp. 1891–1897, Mar. 2017, doi: 10.1007/s10967-016-5160-3.

[34] M. R. Shaltry, R. O. Hoover, and G. L. Fredrickson, "Kinetic Parameters and Diffusivity of Uranium in FLiNaK and ClLiK," *J. Electrochem. Soc.*, vol. 167, no. 11, p. 116502, Jul. 2020, doi: 10.1149/1945-7111/ab9ef0.

[35] C. Moore, W. Doniger, and N. Hoyt, "Assessment of Flow-Enhanced Electrochemical Sensor Testing and Deployments for MSRs," ANL/CFCT-22/34, Sep. 2022.

[36] C. Moore, W. Doniger, and N. Hoyt, "Assessment of Flow-Enhanced Electrochemical Sensor Testing and Deployments for MSRs," ANL/CFCT-23/38, Sep. 2023.
[37] W. H. Doniger, N. A. Shaheen, M. Jubinsky, and N. C. Hoyt, "Quantitative voltammetry measurements of high-concentration actinides in molten chloride fuel salts," *Submitt. J. Electrochem. Soc.*, 2025.
[38] J. C. Imbeaux and J. M. Savéant, "Linear sweep voltammetry. Effect of uncompensated cell resistance and double layer charging on polarization curves," *J. Electroanal. Chem. Interfacial Electrochem.*, vol. 28, no. 2, pp. 325–338, Dec. 1970, doi: 10.1016/S0022-0728(70)80127-9.
[39] N. White and F. Lawson, "Potential sweep voltammetry of metal deposition and dissolution: Part 2. Experimental," *J. Electroanal. Chem. Interfacial Electrochem.*, vol. 26, no. 1, pp. 113–125, Jun. 1970, doi: 10.1016/S0022-0728(70)80069-9.
[40] D. F. Milner and M. J. Weaver, "The influence of uncompensated solution resistance on the determination of standard electrochemical rate constants by cyclic voltammetry, and some comparisons with a.c. voltammetry," *Anal. Chim. Acta*, vol. 198, pp. 245–257, Jan. 1987, doi: 10.1016/S0003-2670(00)85025-4.
[41] N. A. Shaheen, J. Guo, and N. C. Hoyt, "Quantitative Correction of Ohmic Effects on Square Wave Voltammetry for High-Concentration Soluble-Soluble Redox Reactions in Molten Salts," *J. Electrochem. Soc.*, vol. 171, no. 12, p. 126502, Dec. 2024, doi: 10.1149/1945-7111/ad9639.
[42] W. E. Miller and Z. Tomczuk, "Method for making a uranium chloride salt product," Argonne National Laboratory (ANL), Argonne, IL (United States), 6,800,262, Oct. 2004. Accessed: Sep. 22, 2024. [Online]. Available: https://www.osti.gov/doepatents/biblio/935569
[43] R. D. Mariani and D. Vaden, "Modeled salt density for nuclear material estimation in the treatment of spent nuclear fuel," *J. Nucl. Mater.*, vol. 404, no. 1, pp. 25–32, Sep. 2010, doi: 10.1016/j.jnucmat.2010.06.022.
[44] A. Ševčík, "Oscillographic polarography with periodical triangular voltage," *Collect. Czechoslov. Chem. Commun.*, vol. 13, pp. 349–377, 1948, doi: 10.1135/cccc19480349.
[45] J. E. B. Randles, "A cathode ray polarograph. Part II.—The current-voltage curves," *Trans. Faraday Soc.*, vol. 44, no. 0, pp. 327–338, Jan. 1948, doi: 10.1039/TF9484400327.
[46] *COMSOL Multiphysics*®. Stockholm, Sweden. [Online]. Available: www.comsol.com
[47] B. L. Tremillon, "Acid-Base Effects in Molten Electrolytes," in *Molten Salt Chemistry*, in NATO ASI Series. , Springer, Dordrecht, 1987, pp. 279–303. doi: 10.1007/978-94-009-3863-2_14.
[48] B. Li, S. Dai, and D. Jiang, "First-Principles Molecular Dynamics Simulations of UCln–NaCl (n = 3, 4) Molten Salts," *ACS Appl. Energy Mater.*, vol. 2, no. 3, pp. 2122–2128, Mar. 2019, doi: 10.1021/acsaem.8b02157.
[49] D. Inman, G. J. Hills, L. Young, and J. O. Bockris, "Electrode reactions in molten salts: the uranium + uranium trichloride system," *Trans. Faraday Soc.*, vol. 55, no. 0, pp. 1904–1914, Jan. 1959, doi: 10.1039/TF9595501904.
[50] T. A. Johnson, D. V. Laug, S. X. Li, and T. Sofu, "Experimental observations on electrorefining spent nuclear fuel in molten LiCl-KCl/liquid cadmium system.," 3rd International Symposium on New Materials, Montreal, Quebec (CA), 07/04/1999--07/08/1999. Accessed: Sep. 19, 2024. [Online]. Available: https://digital.library.unt.edu/ark:/67531/metadc622283/
[51] B. R. Westphal and R. D. Mariani, "Method for the production of uranium chloride salt," Idaho National Laboratory (INL), Idaho Falls, ID (United States), 8,475,756, Jul. 2013. Accessed: Jun. 21, 2024. [Online]. Available: https://www.osti.gov/doepatents/biblio/1087860
[52] H. Lambert, T. Kerry, and C. A. Sharrad, "Preparation of uranium(III) in a molten chloride salt: a redox mechanistic study," *J. Radioanal. Nucl. Chem.*, vol. 317, no. 2, pp. 925–932, Aug. 2018, doi: 10.1007/s10967-018-5953-7.
[53] Y. Sakamura, T. Inoue, T. Iwai, and H. Moriyama, "Chlorination of UO_2, PuO_2 and rare earth oxides using $ZrCl_4$ in LiCl–KCl eutectic melt," *J. Nucl. Mater.*, vol. 340, no. 1, pp. 39–51, Apr. 2005, doi: 10.1016/j.jnucmat.2004.11.002.

[54] H. Zhang, M. L. Newton, D. E. Hamilton, and M. F. Simpson, "High temperature UCl_3 synthesis in molten salt mixtures via reaction of U metal with iron chlorides," *J. Radioanal. Nucl. Chem.*, vol. 331, no. 1, pp. 383–390, Jan. 2022, doi: 10.1007/s10967-021-08060-9.

[55] C. H. Lee, T.-J. Kim, D. Yoon, J. Jang, G.-Y. Kim, and S.-J. Lee, "Efficient preparation of UCl_3 by $ZnCl_2$ mediated chlorination," *J. Radioanal. Nucl. Chem.*, vol. 322, no. 2, pp. 331–336, Nov. 2019, doi: 10.1007/s10967-019-06782-5.

[56] M. A. Rose, L. D. Gardner, T. T. Lichtenstein, S. A. Thomas, and E. Wu, "Property Measurements of NaCl-UCl_3 and NaCl-KCl-UCl_3 Molten Salts (Rev.1)," Argonne National Laboratory (ANL), Argonne, IL (United States), ANL/CFCT-22/45-Rev.1, May 2023. doi: 10.2172/1985295.

[57] A. Nakayoshi, S. Kitawaki, M. Fukushima, T. Murakami, and M. Kurata, "Investigation of a LiCl–KCl–UCl_3 system using a combination of X-ray diffraction and differential thermal analyses," *J. Nucl. Mater.*, vol. 441, no. 1–3, pp. 468–472, Oct. 2013, doi: 10.1016/j.jnucmat.2013.06.019.

[58] E. Compere, S. Kirslis, E. Bohlmann, F. Blankenship, and W. Grimes, "Fission product behavior in the Molten Salt Reactor Experiment," ORNL--4865, 4077644, Oct. 1975. doi: 10.2172/4077644.

[59] B. R. Harder, G. Long, and W. P. Stanaway, "Compatibility and processing problems in the use of molten uranium chloride - Alkali chloride mixtures as reactor fuels," *Nucl Met Met Soc AIME 15 405-321969*, Dec. 1968, Accessed: Aug. 29, 2025. [Online]. Available: https://www.osti.gov/biblio/4747246

[60] M. G. Chasanov, "Fission-Product Effects in Molten Chloride Fast-Reactor Fuels," *Nucl. Sci. Eng.*, vol. 23, no. 2, pp. 189–190, Oct. 1965, doi: 10.13182/NSE65-A28145.

[61] *HSC Chemistry Software*. Outotec.

[62] "International Target Values for Measurement Uncertainties in Safeguarding Nuclear Materials," International Atomic Energy Agency, STR-368, Sep. 2022. [Online]. Available: https://nucleus.iaea.org/sites/connect/ITVpublic/Resources/International%20Target%20Values%20for%20Measurement%20Uncertainties%20in%20Safeguarding%20Nuclear%20Materials.pdf